Model and form factor dependence in the reaction $ep \to e'K^+\Lambda$

Oren V. Maxwell
Department of Physics, Florida International University, University Park, Miami, Florida 33199, USA
(Received 26 February 2007; published 30 July 2007)

The reaction $ep \to e'K^+\Lambda$ was investigated using a tree-level effective Lagrangian model with coupling parameters fit to empirical cross sections for the reaction $\gamma p \to K^+\Lambda$. The model incorporates both spin $\frac{1}{2}$ and spin $\frac{3}{2}$ resonances in the s and u channels, as well as $K(892)$ and $K(1270)$ resonances in the t channel. Results for the electroproduction cross sections were obtained with four different photoproduction fits, which yield roughly equivalent descriptions of the empirical photoproduction cross sections but which vary in their predictions for photoproduction polarization observables. Electromagnetic form factors are incorporated in a manner similar to previous calculations except that a multiplicative factor is introduced into the masses associated with the s- and u-channel transition form factors so that the sensitivity of the calculated cross sections to these form factors can be studied. Results are presented for the unpolarized differential cross section in a variety of kinematical situations and for particular contributions to the cross section in one particular kinematic situation. The sensitivity of the results to both the photoproduction fit employed and to the transition form factors depends to some extent on the kinematics, but in general, the calculated cross sections are more sensitive to the transition form factors than to the photoproduction fit. Our results suggest that electroproduction data, in conjunction with a reaction model that quantitatively fits the photoproduction data, may provide significant constraints on the electromagnetic form factors associated with resonance excitation.

DOI: 10.1103/PhysRevC.76.014621 PACS number(s): 25.30.Rw, 25.10.+s, 25.20.Lj, 13.60.−r

I. INTRODUCTION

Electromagnetic production of strangeness from protons has been investigated since the mid-1960s, but only comparatively recently has it offered the possibility of yielding fundamental information regarding hadronic and electromagnetic interactions. Both the photoproduction and electroproduction reactions have received experimental attention, but most of the theoretical effort has been concentrated on the photoproduction reaction. Although the photoproduction of kaons from protons is easier to treat theoretically, and is therefore more amenable to a detailed quantitative analysis, the electroproduction reaction is potentially a much richer source of information concerning hadronic and electromagnetic interactions. Not only does electroproduction involve both longitudinal and transverse photons and photons with nonzero squared four-momentum, but in certain kinematical regimes, it depends quite sensitively on the electromagnetic form factors. This suggests that a reaction model that provides a good fit to photoproduction data could be used in conjunction with electroproduction data to study electromagnetic form factors.

A number of experimental studies of the reaction $ep \to e'K^+\Lambda$ were carried out in the early and mid-1970s at Harvard [1], Cornell [2], and DESY [3]. More recent work has been carried out at Jefferson Lab [4–7]. The earliest theoretical studies of kaon electroproduction, dating from the mid-1970s, were based on a fairly simple Regge model [8]. More recent models generally employ an effective tree-level Lagrangian that explicitly incorporates s- and u-channel baryon resonances and a limited number of t-channel kaon resonances [9–13], but there have also been some recent electroproduction calculations based on a Regge model [14]. A number of the more recent calculations have emphasized particular features of the tree-level Lagrangian models as applied to electroproduction, such as the role of the Born terms versus the u-channel resonance contributions [15] and the role of electromagnetic form factors, particularly in the u and t channels [16].

With the exception of Ref. [15], most of the studies based on tree-level Lagrangians fix the model parameters by simultaneously fitting both photoproduction and electroproduction data. Although parameter consistency among all electromagnetic production reactions is certainly a desirable goal, the greater complexity of the electroproduction reaction suggests an alternative procedure. Instead of fitting the photoproduction and electroproduction data simultaneously, one could develop a model fit to just the photoproduction data and then use that model in conjunction with the electroproduction data to study features that are peculiar to electroproduction. For example, by comparing electroproduction results obtained with different photoproduction fits of comparable quality, one might be able to extract some information concerning longitudinal and off-shell photons. By comparing electroproduction results obtained with different form-factor prescriptions, one might be able to extract information concerning the electromagnetic form factors.

The results presented in Ref. [15] represent one step in this direction. In that work, different prescriptions for treating the Born terms and the u-channel resonances were compared. The work presented here represents another step in that direction. We compare the virtual photoproduction cross sections obtained for the reaction $ep \to e'K^+\Lambda$ using four different tree-level Lagrangian models. These four models are modified versions of four of the models described in Ref. [17]. They yield results of comparable quality for the $\gamma p \to K^+\Lambda$ cross sections but give rather different results

for the corresponding polarization parameters. Using two of these models, we also compared results obtained with different choices for the masses in the electromagnetic resonance form factors.

The particular models used to fit the photoproduction cross sections are discussed in Sec. II of this work. All four models are based on the same effective Lagrangian, which includes s-, t-, and u-channel resonance contributions and is similar to that introduced in Ref. [18]. The models were obtained using different starting parameters and differ in the final values obtained for the coupling strengths associated with the various resonances. Only cross section data were employed to generate these fits. At the time the fits were performed, the available polarization data were rather sparse, limited to particular kinematic regions, and of rather limited qualitity. Quite recently the quality and quantity of the available polarization data have increased substantially and should be included in any attempt to quantitatively model the photoproduction process. It should be emphasized, however, that the main purpose of the present study was not to quantitatively fit photoproduction data but to explore to what extent electroproduction and photoproduction data can provide separate information concerning the electromagnetic production of strangeness.

In Sec. III, the extension of the formalism to the electroproduction reaction is considered. Here we also discuss the electromagnetic form factors that are employed in our analysis. Results and discussion are contained in Sec. IV. We find that the different models yield different but not widely dissimilar results for the electroproduction cross sections. However, the sensitivity of the results to the choice of form factor masses can be quite dramatic in certain kinematic regimes.

II. THE REACTION $\gamma p \to K^+\Lambda$

Here we summarize the formalism employed to treat the photoproduction of Λ baryons from protons. Further details may be found in Refs. [17,19]. The various contributions to the reaction are summarized in Fig. 1. In the s channel, the Born contribution is supplemented with contributions with intermediate nucleon resonances. Similarly, the u-channel Born terms are supplemented with contributions with intermediate hyperon resonances, whereas the t-channel Born contribution is supplemented with contributions with intermediate $K^\star(892)$ and $K1(1270)$ resonances.

The list of resonances initially considered in Ref. [17] included all the well-established spin $\frac{1}{2}$ and spin $\frac{3}{2}$ nucleon and hyperon resonances (three- or four-star status) below 1.9 GeV that are listed in the 1998 particle data tables [20]. The restriction to spins less than $\frac{3}{2}$ was imposed mainly for the sake of simplicity. Because there are relatively few well-established resonances below 1.9 GeV with spin greater than $\frac{3}{2}$, it was felt that the additional complexity and parameters required to include higher spin resonances were not warranted. In the course of the fitting procedure, it was found that certain resonances, such as the $\Lambda(1520)$ and the $N(1710)$, had to be excluded to obtain reasonable fits to the empirical cross sections. Certain other resonances, such as the $\Lambda(1810)$, made such negligible contributions to the photoproduction cross section that they could be safely excluded without affecting the results.

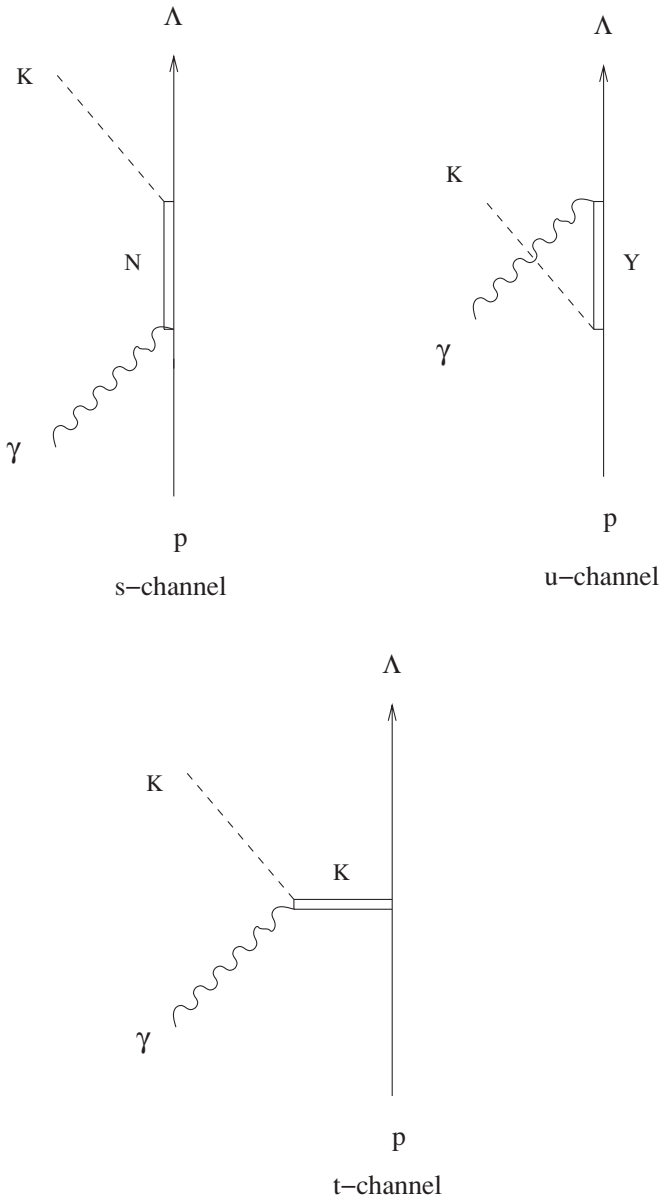

FIG. 1. Contributions to the amplitude for the reaction $\gamma p \to K^+\Lambda$.

The impulse amplitudes depicted in Fig. 1 can be expressed in the general forms

$$\hat{T}_s = \sum_{N^\star} \mathcal{V}_K^\dagger(p_K) D(p_s) \mathcal{V}_\gamma(p_\gamma) \tag{1}$$

$$\hat{T}_u = \sum_{Y^\star} \mathcal{V}_\gamma^\dagger(p_\gamma) D(p_u) \mathcal{V}_K(p_K), \tag{2}$$

and

$$\hat{T}_t = \sum_{K^\star} \mathcal{V}_{\gamma K}^\dagger(p_\gamma, p_t) D_t(p_t) \mathcal{V}_{p\Lambda}(p_t), \tag{3}$$

where $p_s = p_\Lambda + p_K$, $p_u = p_\Lambda - p_\gamma$, and $p_t = p_\gamma - p_K$ are the intermediate four-momenta in the s-, u-, and t-channel

amplitudes, respectively. The $\mathcal{V}$'s here are the vertex functions at the electromagnetic and strong interaction vertices, whereas D and D_t are the intermediate baryon and meson propagators.

In the t channel, the vertex functions are given by the expressions

$$\mathcal{V}_{\gamma K} = e\epsilon \cdot (2p_K - p_\gamma) \tag{4}$$

and

$$\mathcal{V}_{p\Lambda} = g_{\Lambda K p}\gamma_5 \tag{5}$$

for an intermediate ground-state kaon (the t-channel Born term), by

$$\mathcal{V}^\mu_{\gamma K} = \frac{g_{\gamma KK^\star}}{m_{\rm sc}}\epsilon^{\mu\nu\rho\lambda}\epsilon_\nu p_{\gamma\rho} p_{t\lambda} \tag{6}$$

and

$$\mathcal{V}^\mu_{p\Lambda} = \left(g^V_{\Lambda K^\star p} + \frac{g^T_{\Lambda K^\star p}}{m_p + m_\Lambda}\gamma \cdot p_t\right)\gamma^\mu \tag{7}$$

for an intermediate $K^\star(892)$ resonance and by

$$\mathcal{V}^\mu_{\gamma K} = \frac{g_{\gamma KK1}}{m_{\rm sc}}\left(\epsilon \cdot p_t p^\mu_\gamma - p_\gamma \cdot p_t \epsilon^\mu\right) \tag{8}$$

and

$$\mathcal{V}^\mu_{p\Lambda} = \left(g^V_{\Lambda K1p} + \frac{g^T_{\Lambda K1p}}{m_p + m_\Lambda}\gamma \cdot p_t\right)\gamma^\mu\gamma_5 \tag{9}$$

for an intermediate $K1(1270)$ resonance, where $m_{\rm sc}$ is a scaling mass that we set equal to 1000 MeV. The two kaon resonances have propagators of the same form,

$$D_t = \frac{-g_{\mu\nu} + \frac{p_{t\mu}p_{t\nu}}{m^2_{K^\star}}}{p_t^2 - m^2_{K^\star} + im_{K^\star}\Gamma_{K^\star}}, \tag{10}$$

where the label $K^\star$ here refers to either of the two resonances.

The vertex functions and propagators associated with the s and u channels depend on the spin and parity of the intermediate baryon line. For intermediate baryons of spin $\frac{1}{2}$, we employ the standard expression at the electromagnetic vertex and use the pseudoscalar coupling form at the meson vertex. This gives for positive parity baryons

$$\mathcal{V}_{K\frac{1}{2}^+}(p_K) = g\gamma_5 \tag{11}$$

and

$$\mathcal{V}_{\gamma\frac{1}{2}^+}(p_\gamma) = g_\gamma\epsilon_\mu i\sigma^{\mu\nu}(p_\gamma)_\nu \tag{12}$$

with

$$g_\gamma = \frac{e\kappa}{2m_B}, \tag{13}$$

where m_B is the proton mass in the s channel and the Λ mass in the u channel, and κ is defined by its relation to the transition magnetic moment,

$$\mu_T = \frac{e\kappa}{m_B + m_I}. \tag{14}$$

In the last expression m_I denotes the mass of the intermediate baryon. The corresponding expressions for negative parity baryons just have the γ_5 factor transposed from the meson vertex to the electromagnetic vertex. For intermediate protons, there is an additional charge term,

$$\mathcal{V}_{\rm charge}(p_\gamma) = e\gamma^\mu\epsilon_\mu, \tag{15}$$

that has to be added to the positive parity electromagnetic vertex above. For the spin $\frac{1}{2}$ propagator, a relativistic Breit-Wigner form,

$$D^{\frac{1}{2}}(p) = \frac{\gamma \cdot p + m_I}{p^2 - m_I^2 + im_I\Gamma_I}, \tag{16}$$

was used, where Γ_I is the width associated with the intermediate baryon in the s channel and is zero in the u channel.

The correct forms for the propagator and interaction vertices of spin $\frac{3}{2}$ baryons have generated considerable discussion in the literature. On the baryon mass shell, the various prescriptions for the propagator reduce to the Rarita-Schwinger form, which is obtained by multiplying the spin $\frac{1}{2}$ propagator on the right by the projection operator

$$P_{\mu\nu} = g_{\mu\nu} - \frac{1}{3}\gamma_\mu\gamma_\nu + \frac{1}{3}\frac{p_\mu\gamma_\nu - p_\nu\gamma_\mu}{m_I} - \frac{2}{3}\frac{p_\mu p_\nu}{m_I^2}. \tag{17}$$

It is now clear that a correct treatment of the off-shell structure of the spin $\frac{3}{2}$ propagator requires the addition of explicit off-shell terms [21]. The authors of Ref. [12] studied the incorporation of these terms in the electromagnetic production of strangeness from the proton and found them to have a relatively modest effect. In Ref. [17] a comparison was made between photoproduction results obtained with the Rarita-Schwinger propagator and the spin $\frac{3}{2}$ propagator (ABW propagator) introduced in Ref. [18]. There it was found that the propagator choice has a relatively modest influence on the photoproduction cross sections but can have a much more significant effect on certain polarization parameters. The main disadvantage of the ABW propagator is that its use leads to unphysical divergences in the u channel. For that reason, all the results reported here were obtained with the Rarita-Schwinger propagator. Consistent with this propagator choice, we have used

$$\mathcal{V}^\mu_{K\frac{3}{2}^+}(p_K) = -\frac{g}{m_\pi}p^\mu_K, \tag{18}$$

and

$$\mathcal{V}^\mu_{\gamma\frac{3}{2}^+}(p_\gamma) = \left[\frac{g_1}{2m_B}\left(\epsilon^\mu\gamma \cdot p_\gamma - p^\mu_\gamma\gamma \cdot \epsilon\right) + \frac{g_2}{4m_B^2}\left(\epsilon \cdot p_B p^\mu_\gamma - p_\gamma \cdot p_B\epsilon^\mu\right)\right]\gamma_5, \tag{19}$$

for the spin $\frac{3}{2}$ interaction vertices, where p_B is the ground-state baryon four-momentum, and the factor m_π in the first expression makes g dimensionsionless. The negative-parity vertices just have the γ_5 factor transposed from the electromagnetic vertex to the meson vertex.

A. Coupling strengths

To evaluate the various amplitudes discussed above, values are required for the products of the coupling strengths at the two interaction vertices. These coupling products are defined

by the relations

$$\begin{aligned} F_{N^\star} &= e\kappa_{pN^\star} g_{\Lambda K N^\star} \\ F_{\Lambda^\star} &= e\kappa_{\Lambda\Lambda^\star} g_{\Lambda^\star K p} \\ F_{\Sigma^\star} &= e\kappa_{\Lambda\Sigma^\star} g_{\Sigma^\star K p} \end{aligned} \tag{20}$$

for the ground-state baryons and spin $\frac{1}{2}$ resonances in the s and u channels, by

$$\begin{aligned} G^1_{N^\star} &= g_1^{pN^\star} g_{\Lambda K N^\star} \\ G^2_{N^\star} &= g_2^{pN^\star} g_{\Lambda K N^\star} \\ G^1_{\Lambda^\star} &= g_1^{\Lambda\Lambda^\star} g_{\Lambda^\star K p} \\ G^2_{\Lambda^\star} &= g_2^{\Lambda\Lambda^\star} g_{\Lambda^\star K p} \\ G^1_{\Sigma^\star} &= g_1^{\Lambda\Sigma^\star} g_{\Sigma^\star K p} \\ G^2_{\Sigma^\star} &= g_2^{\Lambda\Sigma^\star} g_{\Sigma^\star K p}, \end{aligned} \tag{21}$$

for the spin $\frac{3}{2}$ resonances in the s and u channels, by

$$F_K = e g_{\Lambda K p} \tag{22}$$

for the ground-state kaon in the t channel, and by

$$\begin{aligned} G^V_{K^\star} &= g_{\gamma K K^\star} g^V_{\Lambda K^\star p} \\ G^T_{K^\star} &= g_{\gamma K K^\star} g^T_{\Lambda K^\star p} \end{aligned} \tag{23}$$

for the t-channel kaon resonances. Note in Eqs. (20), that the $N^\star$, $\Lambda^\star$, and $\Sigma^\star$ subscripts refer to either the corresponding ground-state baryon or a spin $\frac{1}{2}$ resonance. For the s- and u-channel Born terms, we also need the coupling products associated with the ground-state baryon charge couplings. These are given by

$$\begin{aligned} F_{Cp} &= e g_{\Lambda K p} \\ F_{C\Lambda} &= e g_{\Lambda K p} \\ F_{C\Sigma} &= e g_{\Sigma K p}. \end{aligned} \tag{24}$$

Only the proton charge coupling contributes to the photoproduction reaction, but all three couplings contribute to the electroproduction reaction.

In Ref. [17], fixed values were adopted for the Born and t-channel coupling products, whereas the s- and u-channel resonance coupling products were adjusted to fit the photoproduction cross-section data. Initial values for the Born couplings were obtained either from the particle data tables [20] or from the well-established πN coupling strength using SU(3) symmetry relations [22]. However, this leads to a value for $g_{\Lambda K p}$ that is much too large to accommodate the empirical photoproduction cross section. To alleviate this difficulty, a reduced value for $g_{\Lambda K p}$ was employed in Ref. [17]. Here we fix the value of $g_{\Sigma K p}$ but allow $g_{\Lambda K p}$ to vary along with the coupling products associated with the s- and u-channel resonances. Together with the fixed Born values, $\kappa_p = 2.793$, $\kappa_\Lambda = -0.729$, and $\kappa_{\Lambda\Sigma} = 1.43$, which were employed in Refs. [17,19], the values of $g_{\Lambda K p}$ and $g_{\Sigma K p}$ completely determine all the Born coupling products.

For the t-channel resonance coupling products, defined by Eqs. (23), we employ the values used in Ref. [17], which were used previously in Ref. [10]. Initial values for the s- and u-channel resonance couplings were obtained using the particle data tables [20] and with the help of SU(3) symmetry relations after assigning the various resonances to particular SU(3) multiplets. The particular SU(3) symmetry assignments are listed in Ref. [17] and discussed more fully in Ref. [19]. The various coupling products were then varied to fit an empirical representation of the $\gamma p \to K^+\Lambda$ cross-section data generated by the Virginia Tech Partial-Wave Analysis Facility (SAID) [23]. In particular, the SAID photoproduction cross sections at laboratory photon energies of 1.1, 1.4, and 1.7 GeV were fit by minimizing the cumulative error parameter defined by

$$\chi^2 = \sum \frac{(d\sigma_{\rm calc} - d\sigma_{\rm emp})^2}{\bar{d\sigma}^2}, \tag{25}$$

where the sum is carried out over the three energies and several angles for each energy and $\bar{d\sigma}^2$ is the angle average of $d\sigma^2_{\rm emp}$ at each energy.

The coupling constant products associated with the resulting fits are listed in Table I. These fits differ from those discussed in Ref. [17] in three respects. First, they include the t-channel Born term, which was not included in the fits of Ref. [17]. Second, as discussed above, the value of $g_{\Lambda K p}$ was varied rather than held fixed. Finally, the fits presented here were obtained with an improved fitting routine that yielded cumulative χ^2 values significantly lower than those obtained with the fits of Ref. [17]. Because of these lower χ^2 values, one might have expected the corresponding polarization parameters to exhibit less variation among the fits than was reported in Ref. [17], but, as will be discussed in Sec. IV, this was not the case.

As mentioned in the introduction, the four different fits shown in Table I were obtained with four different sets of starting parameters. As can be seen, quite different values for the final coupling products were obtained for some of the resonances in the different fits. No particular physical significance should be attached to these differences. The fits do not differ in any particular physical property that distinguishes one fit from another, except that in fit D, the spin $\frac{3}{2}$ resonances have been suppressed. The different results obtained for the coupling products just reflect the fact that cross section data alone do not completely constrain the parameters of the photoproduction model. The χ^2 values obtained for fits A and B are nearly the same, whereas those associated with fits C and D are about a factor 4 to 5 higher than those of fits A and B.

B. s-channel resonance widths

In addition to the coupling strength products, values are required for the nucleon resonance widths to evaluate the s-channel amplitude. These widths are generally required at positions rather far off the mass shells. To treat the off-shell structure of the resonance widths, we employ a dynamical model introduced in Ref. [19] and used in Ref. [17] in which the full widths are decomposed into a number of partial widths for decay into particular two- and three-body channels. In each such channel, the off-shell energy and momentum dependence is treated using an effective Lagrangian model

TABLE I. Coupling constant products. The four fits shown here correspond to four different sets of starting parameters. Fits A and B yield similar values of χ^2; fits C and D yield χ^2 values that are about a factor of 4 to 5 higher.

		A	B	C	D
		Spin $\frac{1}{2}$ resonances			
N	F_p	−4.3391	−4.2928	−2.6060	−4.1952
	F_{Cp}	−1.5535	−1.5370	−0.9330	−1.5020
$N(1440)$	$F_{N^\star}$	0.4345	−7.1660	6.7908	1.1553
$N(1535)$	$F_{N^\star}$	−0.5915	−0.1424	0.4886	−1.8045
$N(1650)$	$F_{N^\star}$	0.0901	−0.0527	−0.0082	0.5368
Λ	F_Λ	1.1325	1.1205	0.6802	1.0950
	$F_{C\Lambda}$	−1.5535	−1.5370	−0.9330	−1.5020
$\Lambda(1405)$	$F_{\Lambda^\star}$	−1.1545	−3.3238	1.9185	−2.6032
$\Lambda(1600)$	$F_{\Lambda^\star}$	−9.9890	0.0760	−9.2695	−5.5547
$\Lambda(1670)$	$F_{\Lambda^\star}$	0.3646	−2.9309	−4.6396	−0.7691
Σ	F_Σ	1.4579	1.4579	1.4579	1.4579
	$F_{C\Sigma}$	1.0195	1.0195	1.0195	1.0195
$\Sigma(1660)$	$F_{\Sigma^\star}$	4.7058	−4.3533	8.6511	4.1221
$\Sigma(1750)$	$F_{\Sigma^\star}$	2.9912	9.8805	8.0686	−0.0210
		Spin $\frac{3}{2}$ resonances			
$N(1520)$	$G^1_{N^\star}$	−0.3546	−0.4698	−0.6468	−0.7542
	$G^2_{N^\star}$	0.5680	0.0402	−1.4321	−0.5632
$N(1700)$	$G^1_{N^\star}$	1.1898	1.0531	0.5569	0.4107
	$G^2_{N^\star}$	1.2593	1.1681	0.6676	0.5098
$N(1720)$	$G^1_{N^\star}$	0.0223	0.0153	−0.0093	0.0716
	$G^2_{N^\star}$	0.1902	0.1986	−0.2517	0.2545
$\Lambda(1690)$	$G^1_{\Lambda^\star}$	9.1950	−0.3376	8.2806	0
	$G^2_{\Lambda^\star}$	−7.3240	−7.4468	1.6828	0
$\Lambda(1890)$	$G^1_{\Lambda^\star}$	2.3565	2.0982	0.3954	0
	$G^2_{\Lambda^\star}$	−9.8617	−9.8317	−9.9899	0
$\Sigma(1385)$	$G^1_{\Sigma^\star}$	−0.8835	−0.8494	0.0718	0
	$G^2_{\Sigma^\star}$	5.3331	5.0737	4.5280	0
$\Sigma(1670)$	$G^1_{\Sigma^\star}$	−8.1875	1.1902	−8.4442	0
	$G^2_{\Sigma^\star}$	9.6711	9.7155	−1.7887	0
		t-channel resonances			
K	F_K	1.5535	1.5370	0.9330	1.5020
$K(892)$	$G^V_{K^\star}$	−2.0100	−2.0100	−2.0100	−2.0100
	$G^T_{K^\star}$	1.0000	1.0000	1.0000	1.0000
$K(1270)$	$G^V_{K^\star}$	0.2500	0.2500	0.2500	0.2500
	$G^T_{K^\star}$	2.1300	2.1300	2.1300	2.1300

with the required coupling strength adjusted to yield the empirical on-shell branching ratio for decay into that channel.

Within this scheme, the two-body channels all involve the decay of a nucleon resonance into a pseudoscalar meson and a spin $\frac{1}{2}$ ground-state baryon. In the resonance rest frame, the corresponding widths are given by

$$\Gamma\left(\frac{1}{2}^P \to \frac{1}{2}^+ + 0^-\right) = \frac{f^2}{4\pi}\frac{p}{\sqrt{s}}[E_B - \eta_P m_B] \quad (26)$$

TABLE II. $N^\star$ resonance on-shell branching ratios.

Resonance	Two body channels			Three body channels		
	$N\pi$	$N\eta$	ΛK	$N\rho$	$N\sigma$	$\Delta(1232)\pi$
$N(1440)$	0.65			0.10		0.25
$N(1520)$	0.55			0.20	0.05	0.20
$N(1535)$	0.45	0.50		0.03	0.02	
$N(1650)$	0.75	0.06	0.06	0.08		0.05
$N(1700)$	0.10	0.017		0.063	0.22	0.60
$N(1710)$	0.15	0.01	0.15		0.26	0.43
$N(1720)$	0.15	0.012	0.07	0.768		

for spin $\frac{1}{2}$ resonances and by

$$\Gamma\left(\frac{3}{2}^P \to \frac{1}{2}^+ + 0^-\right) = \frac{1}{12\pi}\frac{f^2}{m_\pi^2}\frac{p^3}{\sqrt{s}}[E_B + \eta_P m_B], \quad (27)$$

for spin $\frac{3}{2}$ resonances, where P specifies the resonance parity, p is the channel momentum, E_B is the energy of the baryon decay product, and η_P is $+1$ or -1 for even- or odd-parity resonances, respectively. If the threshold for a particular channel lies above the resonance center-of-mass energy, then that channel is omitted.

That part of the on-shell decay width not accounted for by two-body channels is assigned to three-body channels, which are treated approximately as either a decay into a ground-state baryon and a meson resonance or as a decay into a ground-state meson and a baryon resonance. In particular, we include decays into the $N\rho$, $N\sigma$, and $\Delta(1232)\pi$ channels. Branching ratios for all the nucleon resonances included in this work are listed in Table II. The values given there for the two-body channels, as well as some of the three-body channels, were obtained from the particle data tables [20]. After adding together all the branching ratios for which data exists, any remaining decay width still not accounted for was assigned to whatever other channels are open for that resonance.

For decays into unstable mesons or baryons, a method was developed in Ref. [19] for handling the widths of the decay products. The same method was used in the present work. Briefly, the method requires the replacement of the unstable decay product mass in the width expression by a variable mass parameter and then integration of the resulting phase-space factor multiplied by a Breit-Wigner distribution function. Detailed expressions are given in Ref. [19]. For each resonance, the partial widths are normalized to yield the empirical value for the total width at the on-shell position of the resonance.

C. Matrix elements and observables

For the reaction $\gamma p \to K^+\Lambda$, the baryon matrix elements of the reaction amplitude all have the general structure

$$\bar{u}_{M_\Lambda}(p_\Lambda)\hat{T}u_{M_p}(p_p) = \bar{u}_{M_\Lambda}(p_\Lambda)\left[\hat{A} + \hat{B}\gamma_5 + \hat{C}\gamma^0 + \hat{D}\gamma^0\gamma_5\right]u_{M_p}(p_p), \quad (28)$$

where p_p and M_p are the four-momentum and spin projection of the proton, and p_Λ and M_Λ the four-momentum and spin

projection of the Λ. The structures of the operators $\hat{A}$, $\hat{B}$, $\hat{C}$, and $\hat{D}$ depend on the spin and parities associated with the particular contributions considered. Detailed expressions for them have been collected in an appendix of Ref. [19].

Equation (28) can be either evaluated directly or converted to the equivalent Pauli form,

$$\begin{aligned}\bar{u}_{M_\Lambda}(p_\Lambda)\hat{T}u_{M_p}(p_p) &= N_\Lambda N_p \chi^\dagger_{M_\Lambda}[(\hat{A}+\hat{C})+(\hat{B}+\hat{D})\sigma\cdot\hat{p}_p \\ &\quad +\sigma\cdot\hat{p}_\Lambda(\hat{D}-\hat{B})+\sigma\cdot\hat{p}_\Lambda(\hat{C}-\hat{A})\sigma\cdot\hat{p}_p]\chi_{M_p} \end{aligned} \quad (29)$$

with

$$N=\sqrt{\frac{E+m}{2m}} \quad (30)$$

and

$$\hat{p}=\frac{\mathbf{p}}{E+m}. \quad (31)$$

This last expression can be further reduced analytically, but the procedure is rather tedious. Instead, Eq. (29) was evaluated numerically. As a check on the resulting matrix elements, an independent code was written to evaluate Eq. (28) numerically and the results were compared with those of the Pauli numerical evaluation.

The unpolarized differential cross section for the reaction $\gamma p \to K^+\Lambda$ is given in the center-of-mass (c.m.) by

$$\frac{d\sigma}{d\Omega}=\frac{1}{(2\pi)^2}\frac{m_p m_\Lambda p_F}{4E_\gamma s}\frac{1}{4}\sum_{\text{spins}}|\langle F|\hat{T}|I\rangle|^2, \quad (32)$$

where p_F is the magnitude of the outgoing three-momentum, s is the squared total energy in the center-of-mass, and E_γ is the incident photon energy. In addition to the unpolarized cross section, we have also obtained results for the hyperon polarization asymmetry P, the polarized photon beam asymmetry Σ, and the polarized proton target asymmetry T defined by

$$P=\frac{d\sigma^+_\Lambda-d\sigma^-_\Lambda}{d\sigma^+_\Lambda+d\sigma^-_\Lambda}, \quad (33)$$

$$\Sigma=\frac{d\sigma^\perp_\gamma-d\sigma^\parallel_\gamma}{d\sigma^\perp_\gamma+d\sigma^\parallel_\gamma}, \quad (34)$$

and

$$T=\frac{d\sigma^+_p-d\sigma^-_p}{d\sigma^+_p+d\sigma^-_p}, \quad (35)$$

where the superscripts $^+$ and $^-$ refer to spin projections above and below the scattering plane, i.e., along the positive and negative y axes, respectively, and the superscripts $^\perp$ and $^\parallel$ refer to photon polarizations perpendicular and parallel to the scattering plane, respectively.

III. THE REACTION $ep \to e'K^+\Lambda$

Figure 2 depicts the reaction amplitude for the electroproduction of a Λ from a proton. The large circle on the baryon line here represents the various s-channel, u-channel, and

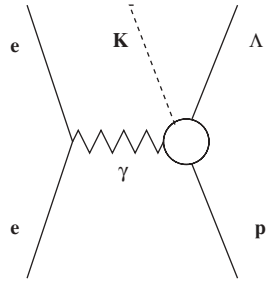

FIG. 2. The amplitude for the reaction $ep \to e'K^+\Lambda$.

t-channel amplitudes depicted in Fig. 1. The corresponding matrix element is most conveniently expressed in the form,

$$\langle F|\hat{T}|I\rangle=\frac{l_\mu h^\mu}{q^2}, \quad (36)$$

where q^2 is the squared four-momentum of the exchanged virtual photon, l_μ is the lepton current given by

$$l_\mu = e\bar{u}_{M'}(p')\gamma_\mu u_M(p), \quad (37)$$

and h^μ is the hadron current that has the general form

$$h_\mu = e\bar{u}_{M_\Lambda}(p_\Lambda)\hat{t}_\mu u_{M_p}(p_p). \quad (38)$$

In the lepton current, p and p' are the incident and final electron four-momenta and M and M' the corresponding spin projections.

The square of this matrix element has to be averaged over the initial electron and proton spins and summed over the final electron and Λ spins. The sum over lepton spins can be performed analytically, yielding the result

$$\frac{1}{4}\sum_{\text{spins}}|\langle F|\hat{T}|I\rangle|^2=\frac{e^2}{4m_e^2q^4}\sum_{M_\Lambda M_p}\left[\frac{1}{2}q^2|h|^2+2(p\cdot h)^2\right], \quad (39)$$

where the factor $\frac{1}{4}$ on the left arises from the average over the initial electron and proton spins. Using current conservation, $q_\mu h^\mu = 0$, permits this to be reduced, in the extreme relativistic limit for the electrons, to the form

$$\frac{1}{4}\sum_{\text{spins}}|\langle F|\hat{T}|I\rangle|^2=\frac{e^2}{2m_e^2q^2}\frac{1}{\epsilon-1}\sum_{M_\Lambda M_p}\frac{1}{2}|\langle f|\hat{t}_\gamma|i\rangle|^2, \quad (40)$$

where $\langle f|\hat{t}_\gamma|i\rangle$ is the matrix element for the virtual photoproduction of a Λ from a proton and ε, the transverse polarization of the virtual photon, is given by

$$\epsilon=\left(1-2\frac{\mathbf{q}^2}{q^2}\tan^2\frac{\Psi}{2}\right)^{-1}. \quad (41)$$

with Ψ denoting the electron scattering angle.

The differential electroproduction cross section has the form

$$\frac{d\sigma}{dE'd\Omega'd\Omega_K}=\frac{1}{(2\pi)^5}\frac{m_e^2m_pm_\Lambda p'p_K^2}{2E_\Lambda E_K R\sqrt{(p_\mu p_p^\mu)^2-m_e^2m_p^2}}\times\frac{1}{4}\sum_{\text{spins}}|\langle F|\hat{T}|I\rangle|^2, \quad (42)$$

where the factor R is given by

$$R = \frac{\mathbf{p_K}}{p_K}\left(\frac{\mathbf{p_K}}{E_K} - \frac{\mathbf{p}_\Lambda}{E_\Lambda}\right), \tag{43}$$

and now p' and p_K denote the magnitudes of the outgoing electron and kaon three-momenta. In the extreme relativistic electron limit, this can be reexpressed as

$$\frac{d\sigma}{dE'd\Omega' d\Omega_K} = \frac{\alpha}{(2\pi)^4}\frac{p'}{(\epsilon-1)q^2}\sqrt{\frac{\left(q_\mu p_p^\mu\right)^2 - q^2 m_p^2}{\left(p_\mu p_p^\mu\right)^2 - m_e^2 m_p^2}}\frac{d\sigma_\gamma}{d\Omega_K}, \tag{44}$$

where α is the fine structure constant, and

$$\frac{d\sigma_\gamma}{d\Omega_K} = \frac{1}{(4\pi)^2}\frac{m_p m_\Lambda p_K^2}{E_\Lambda E_K R\sqrt{\left(q_\mu p_p^\mu\right)^2 - q^2 m_p^2}}\frac{1}{2}\sum_{\text{spins}}|\langle f|\hat{t}_\gamma|i\rangle|^2, \tag{45}$$

is the differential cross section for virtual photoproduction. In the $K\Lambda$ center-of-mass system, the latter quantity reduces to

$$\frac{d\sigma_\gamma}{d\Omega_K} = \frac{1}{(4\pi)^2}\frac{m_p m_\Lambda p_K}{|\mathbf{q}|s}\frac{1}{2}\sum_{\text{spins}}|\langle f|\hat{t}_\gamma|i\rangle|^2, \tag{46}$$

where $\sqrt{s} = E_K + E_\Lambda$ in the $K\Lambda$ center-of-mass system. Alternatively,

$$\frac{d\sigma_\gamma}{dt} = \frac{1}{16\pi}\frac{m_p m_\Lambda}{|\mathbf{q}|^2 s}\frac{1}{2}\sum_{\text{spins}}|\langle f|\hat{t}_\gamma|i\rangle|^2, \tag{47}$$

with $t = (p_K - q)^2$.

A. Virtual photoproduction matrix elements

The spin-summed squared matrix element for virtual photoproduction of a Λ is most simply written in a coordinate system defined with respect to the lepton plane. In particular, with the z axis defined in the direction of the virtual photon three-momentum and the x axis defined so that $\mathbf{p}$ lies in the xz plane, we have

$$\frac{1}{2}\sum_{\text{spins}}|\langle f|\hat{t}_\gamma|i\rangle|^2 = \frac{1}{2}\sum_{M_\Lambda M_p}\left[\frac{1}{2}(\epsilon+1)|h_x|^2 - \frac{1}{2}(\epsilon-1)|h_y|^2 + \epsilon_L|h_z|^2 - \sqrt{2\epsilon_L(\epsilon+1)}\Re(h_x h_z^\star)\right], \tag{48}$$

where ϵ_L, the longitudinal polarization of the virtual photon, is related to the transverse polarization by

$$\epsilon_L = -\frac{q^2}{q_0^2}\epsilon, \tag{49}$$

with q_0 denoting the fourth component of the virtual photon four-momentum. Note here that the squared four-momentum, q^2, is negative.

Although the expression for the spin-summed squared matrix element is simplest in a coordinate system defined with respect to the lepton plane, the hadron current components are most easily evaluated in a coordinate system defined with respect to the hadron plane. If we let the z axes of the two coordinate systems coincide and let the x axis of the hadronic system be defined so that $\mathbf{p_K}$ lies in the xz plane, then the components of the hadron current in the two coordinate systems are related by a simple rotation. In particular,

$$\begin{aligned} h_x &= \tilde{h}_x\cos\phi - \tilde{h}_y\sin\phi \\ h_y &= \tilde{h}_x\sin\phi + \tilde{h}_y\cos\phi \\ h_z &= \tilde{h}_z, \end{aligned} \tag{50}$$

where the $\tilde{h}$ are the components of the hadron current in the hadronic coordinate system and ϕ is the angle between the hadron plane and the lepton plane.

After carrying out the Dirac algebra, the hadron current takes the general form

$$\begin{aligned} \tilde{\mathbf{h}} = \chi^\dagger_{M_\Lambda}[&Ai\mathbf{p_K}\times\mathbf{q} + (B_1\mathbf{q} + B_2\mathbf{p_K})\sigma\cdot\mathbf{p_K} \\ &+ (C_1\mathbf{q} + C_2\mathbf{p_K})\sigma\cdot\mathbf{q} + D\sigma + Ei\mathbf{p_K} \\ &\times\mathbf{q}\sigma\cdot i\mathbf{p_K}\times\mathbf{q}]\chi_{M_p}, \end{aligned} \tag{51}$$

where the coefficients A, B_1, B_2, C_1, C_2, D, and E depend on the particular s-channel, u-channel, or t-channel contribution considered. In terms of these coefficients, the virtual photoproduction cross section can be decomposed in the usual manner,

$$\begin{aligned} \frac{d\sigma_\gamma}{d\Omega_K} = \frac{d\sigma_U}{d\Omega_K} + \epsilon_L\frac{d\sigma_L}{d\Omega_K} + \epsilon\frac{d\sigma_P}{d\Omega_K}\sin^2\theta\cos 2\phi \\ + \sqrt{2\epsilon_L(\epsilon+1)}\frac{d\sigma_I}{d\Omega_K}\sin\theta\cos\phi, \end{aligned} \tag{52}$$

where θ is the angle between the three-momenta of the virtual photon and the outgoing kaon in the $K\Lambda$ center-of-mass system, and

$$\begin{aligned} \frac{d\sigma_U}{d\Omega_K} &= k|D|^2 + \frac{1}{2}k(\zeta_2 + \xi_1|\mathbf{q}|^2)|\mathbf{p_K}|^2\sin^2\theta \\ \frac{d\sigma_L}{d\Omega_K} &= k(|D|^2 + \zeta_1|\mathbf{q}|^2 + \zeta_2|\mathbf{p_K}|^2\cos^2\theta + 2\xi_2|\mathbf{p_K}||\mathbf{q}|\cos\theta) \\ \frac{d\sigma_P}{d\Omega_K} &= \frac{1}{2}k(\zeta_2 - \xi_1|\mathbf{q}|^2)|\mathbf{p_K}|^2 \\ \frac{d\sigma_I}{d\Omega_K} &= -k(\zeta_2|\mathbf{p_K}|^2\cos^2\theta + \xi_2|\mathbf{p_K}||\mathbf{q}|) \end{aligned} \tag{53}$$

with

$$k = \frac{m_p m_\Lambda}{16\pi|\mathbf{q}|^2 s}, \tag{54}$$

$$\zeta_1 = |B_1\mathbf{p_K} + C_1\mathbf{q}|^2 + 2\Re(C_1 D^\star), \tag{55}$$

$$\zeta_2 = |B_2\mathbf{p_K} + C_2\mathbf{q}|^2 + 2\Re(B_2 D^\star), \tag{56}$$

$$\xi_1 = |A|^2 + |E|^2|\mathbf{p_K}\times\mathbf{q}|^2 - 2\Re(ED^\star), \tag{57}$$

and

$$\xi_2 = \Re[(B_1\mathbf{p_K} + C_1\mathbf{q})\cdot(B_2\mathbf{p_K} + C_2\mathbf{q})^\star + (B_1 + C_2)D^\star]. \tag{58}$$

Detailed expressions for the coefficients A, B_1, B_2, C_1, C_2, D, and E are given in the appendix. It should be noted that although the decomposition given by Eq. (52) has frequently been employed by theorists, experimentalists generally prefer a form that has a factor ε multiplying the longitudinal term rather than ϵ_L.

To check the algebra leading to the equations above, we wrote independent numerical codes that evaluate the virtual photoproduction cross section using either the decomposition Eq. (53) or Eq. (46) directly and then compared the results for different kinematical situations. This procedure checks not only the relevant algebra but also the numerical codes themselves. As a check on the hadronic matrix elements, we have also compared the results of independent codes that either make use of the Pauli reduction, Eq. (51), or evaluate the Dirac matrix elements numerically.

B. Electromagnetic form factors

To take account of the off-shell nature of the virtual photon in electroproduction, the matrix elements discussed above must be supplemented by electromagnetic form factors. In the strange particle sector there is relatively little information concerning these form factors. Nor is there much information concerning the electromagnetic form factors of nucleon resonances. Indeed, as mentioned in the introduction, it is to be hoped that a careful analysis of electroproduction, using a model fit to photoproduction data, might yield significant constraints on the electromagnetic form factors of both strange particles and baryon and kaon resonances.

The sensitivity of electroproduction observables to the t-channel electromagnetic form factors has been studied extensively by the authors of Ref. [11]. They found that the unpolarized cross section, given by

$$\frac{d\sigma_{UL}}{d\Omega_K} = \frac{d\sigma_U}{d\Omega_K} + \epsilon_L \frac{d\sigma_L}{d\Omega_K}, \tag{59}$$

is relatively insensitive to the t-channel form factors, but that the individual contributions to Eq. (52), especially the interference term, can be quite sensitive to these form factors. Similar results have been reported in Ref. [24]. Here we focus more on the sensitivity of electroproduction results to the s- and u-channel form factors. We adopt fixed form factors in the t channel but allow the mass scales associated with the resonance form factors in the s and u channels to vary by an overall multiplicative factor. Although not well motivated by any fundamental considerations, this simple procedure allows us to investigate, in a very basic way, how sensitive the virtual photoproduction cross section is to the baryon resonance form factors.

In the t channel we employ form factors that were among those considered in Ref. [11]. In particular, a parametrization is used for the $\gamma K K$ form factor that is based on a relativistic constituent quark model [25]. It has the form

$$F_K(q^2) = \alpha_K \frac{\Lambda_1^2}{\Lambda_1^2 - q^2} + (1-\alpha_K)\left(\frac{\Lambda_2^2}{\Lambda_2^2 - q^2}\right)^2 \tag{60}$$

with $\alpha_K = 0.398$, $\Lambda_1 = 0.642$ GeV, and $\Lambda_2 = 1.386$ GeV. For the kaon resonance transition form factors, parametrizations based on a vector dominance model [9] are used. These have the form

$$F_{K^\star}(q^2) = \frac{\Lambda_{K^\star}^2}{\Lambda_{K^\star}^2 - q^2} \tag{61}$$

with $\Lambda_{K^\star} = 0.95$ GeV for the $\gamma K K(892)$ vertex and $\Lambda_{K^\star} = 0.55$ GeV for the $\gamma K K(1270)$ vertex. Note that these t-channel form factors are all normalized to unity at the physical photon point, $q^2 = 0$.

In the s and u channels, we adopt a prescription used in several previous studies [10–12] but modified by the inclusion of a multiplicative factor in the masses of the resonance form factors. This prescription is based on the extended vector meson dominance model (EVMD model) developed in Ref. [26] for the nucleon electromagnetic form factors in which the usual vector dominance terms are supplemented with a perturbative QCD term. Within this model, the charge and magnetic form factors are decomposed in the usual way

$$\begin{aligned} F_C(q^2) &= F_1(q^2) + \tau F_2(q^2) \\ F_M(q^2) &= \frac{1}{\kappa}[F_1(q^2) + F_2(q^2)], \end{aligned} \tag{62}$$

where

$$\tau = \frac{q^2}{4m_p^2}, \tag{63}$$

and κ is the dimensionless anomalous magnetic moment of either the proton or the neutron. The form factors F_1 and F_2 have both isoscalar and isovector contributions. In particular,

$$\begin{aligned} F_1(q^2) &= \tfrac{1}{2}[F_{1S}(q^2) \pm F_{1V}(q^2)] \\ F_2(q^2) &= \tfrac{1}{2}[\kappa_S F_{2S}(q^2) \pm \kappa_V F_{2V}(q^2)], \end{aligned} \tag{64}$$

where the sign is positive for protons and negative for neutrons, and the isoscalar and isovector magnetic moment factors, κ_S and κ_V, are defined by their relations with the proton and neutron magnetic moments,

$$\begin{aligned} \kappa_S &= \kappa_p + \kappa_n - 1 \\ \kappa_V &= \kappa_p - \kappa_n - 1. \end{aligned} \tag{65}$$

Using the values $\kappa_p = 2.793$ and $\kappa_n = -1.913$ [20] in the latter expressions yields $\kappa_S = -0.12$ and $\kappa_V = 3.706$.

The EVMD model attributes the isoscalar form factor to ω exchange modified by a perturbative QCD term and the isovector form factor to ρ exchange modified by the same quantum chromodynamics (QCD) term. The authors of Ref. [26] employ the forms

$$\begin{aligned} F_{iS}(q^2) &= \alpha_{i\omega}\frac{m_\omega^2}{m_\omega^2 - q^2}F_{i\omega}(q^2) + (1-\alpha_{i\omega})F_{iD}(q^2) \\ F_{iV}(q^2) &= \alpha_{i\rho}\frac{m_\rho^2}{m_\rho^2 - q^2}F_{i\rho}(q^2) + (1-\alpha_{i\rho})F_{iD}(q^2) \end{aligned} \tag{66}$$

for $i = 1$ or $i = 2$, with $m_\omega = 0.783$ GeV, $m_\rho = 0.770$ GeV, and

$$\begin{aligned} \alpha_{1\omega} &= \frac{g_\omega}{f_\omega} = 0.658 \\ \alpha_{2\omega} &= \frac{\kappa_\omega}{\kappa_S}\alpha_{1\omega} = -2.19 \\ \alpha_{1\rho} &= \frac{g_\rho}{f_\rho} = 0.631 \\ \alpha_{2\rho} &= \frac{\kappa_\rho}{\kappa_V}\alpha_{1\rho} = 0.562. \end{aligned} \tag{67}$$

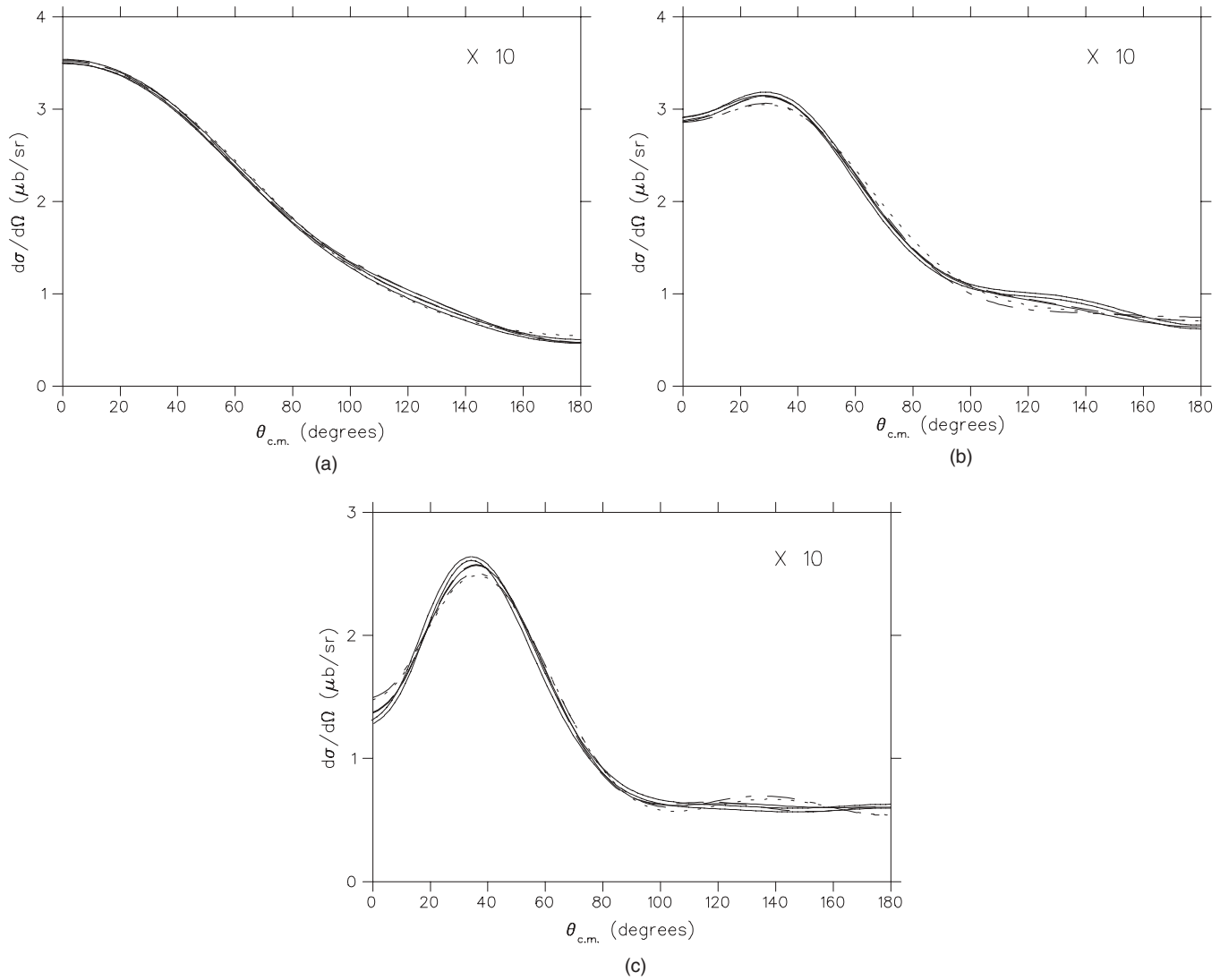

FIG. 3. Differential cross section for the reaction $\gamma p \to K^+\Lambda$ at (a) $E_\gamma = 1.1$ GeV, (b) $E_\gamma = 1.4$ GeV, and (c) $E_\gamma = 1.7$ GeV. The solid curves were obtained with fit A, the dashed curves with fit B, the dotted curves with fit C, and the dot-dashed curves with fit D, as described in the text. The double solid curves are empirical fits from Ref. [23].

The functions F_i appearing on the right sides of Eqs. (66) are given by

$$F_{1\alpha}(q^2) = \frac{\Lambda_{1\alpha}^2}{\Lambda_{1\alpha}^2 - \tilde{q}^2}\frac{\Lambda_2^2}{\Lambda_2^2 - \tilde{q}^2}$$
$$F_{2\alpha}(q^2) = \frac{\Lambda_{1\alpha}^2}{\Lambda_{1\alpha}^2 - \tilde{q}^2}F_{1\alpha}(q^2), \tag{68}$$

with

$$\tilde{q}^2 = q^2\frac{\ln\frac{\Lambda_2^2 - q^2}{\Lambda_{\rm QCD}^2}}{\ln\frac{\Lambda_2^2}{\Lambda_{\rm QCD}^2}}, \tag{69}$$

and in the most recent (1992) fit, $\Lambda_{1\omega} = \Lambda_{1\rho} = 0.863$ GeV, $\Lambda_{1D} = 1.21$ GeV, $\Lambda_2 = 2.1$ GeV, and $\Lambda_{\rm QCD} = 0.33$ GeV. Note that the isoscalar and isovector form factors are normalized so that in the limit $q^2 \to 0$, $F_{1p} \to 1$, $F_{2p} \to \kappa_p - 1$, $F_{1n} \to 0$, and $F_{2n} \to \kappa_n$. This ensures that in the same limit, by virtue of Eqs. (62), F_C reduces to unity for protons and zero for neutrons, and F_M reduces to unity for both protons and neutrons, thereby yielding nucleon electromagnetic couplings that have the correct empirical strengths at the physical photon point.

Following Refs. [10–12], we assume that all neutral ground-state baryons are governed by the same electromagnetic form factors so that in the u-channel Born terms, we set the charge and magnetic form factors equal to the corresponding neutron form factors suitably normalized, as discussed above. However, as mentioned in Ref. [16], this may yield a Λ magnetic form factor with the wrong q^2 dependence. Although the chiral quark-soliton model [27] does yield a Λ form factor that mimics that of the neutron, another model, the hybrid vector meson dominance model [28], yields a Λ form factor that significantly exceeds the neutron form factor at negative values of q^2. If the latter model is correct, then the universality assumption for the form factors of neutral ground-state baryons

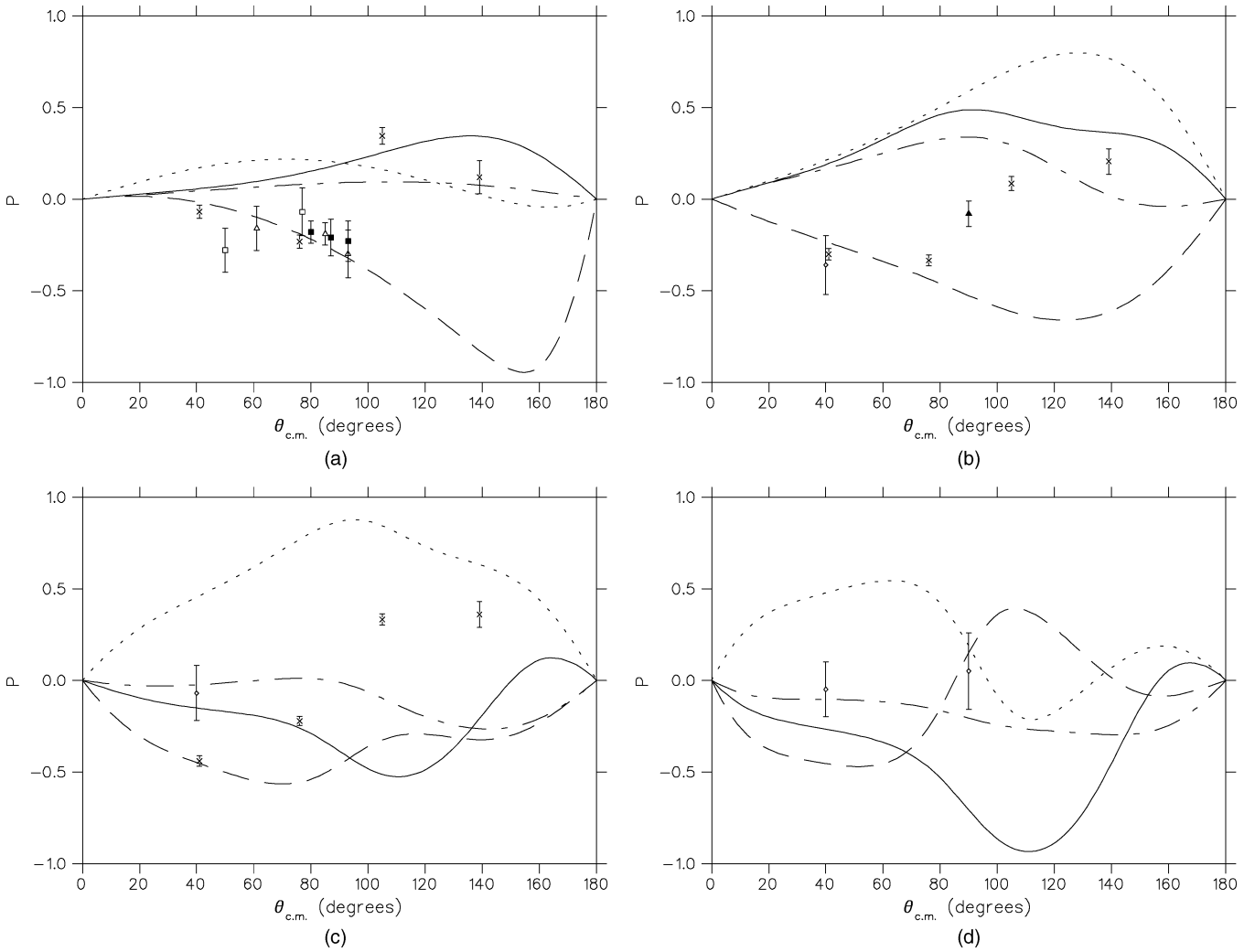

FIG. 4. Hyperon polarization asymmetry for the reaction $\gamma p \to K^+\Lambda$ at (a) $E_\gamma = 1.0$ GeV, (b) $E_\gamma = 1.25$ GeV, (c) $E_\gamma = 1.55$ GeV, and (d) $E_\gamma = 1.7$ GeV. Identification of curves as described in the legend to Fig. 3. The data points are from Ref. [29] (solid squares), Ref. [30] (open triangles), Ref. [31] (open squares), Ref. [32] (solid triangles), Ref. [33] (open diamonds), and Ref. [34] (crosses).

may overestimate the u-channel Born contributions to the virtual photoproduction of strangeness.

For the s- and u-channel resonance contributions, the usual prescription [10–12] is to assume that all positively charged resonances are governed by one electromagnetic transition form factor, which is set equal to the second form factor of the proton, F_{2p}, suitably normalized, and that all neutral resonances are governed by one other transition form factor, which is set equal to the second form factor of the neutron, F_{2n}. This prescription has the virtue of simplicity but does not really have any compelling theoretical justification other than the universality hypothesis for the vector-meson couplings. Here we make a modification to the usual prescription that allows us to investigate in a simple way the sensitivity of electroproduction observables to the electromagnetic resonance form factors. As in previous work [10–12], we employ single transition form factors for all positively charged resonances and for all neutral resonances, but we introduce a multiplicative factor in the masses associated with these form factors; i.e., we replace the resonance form-factor masses appearing in Eqs. (68) and (69) by

$$\begin{aligned} \tilde{\Lambda}_{1\alpha} &= c_R \Lambda_{1\alpha} \\ \tilde{\Lambda}_{2\alpha} &= c_R \Lambda_{2\alpha} \end{aligned} \tag{70}$$

and then study the resulting cross sections as a function of the multiplicative factor c_R. With this modification, the properly normalized transition form factors are

$$F_{N^\star}(q^2) = \frac{\tilde{F}_{2p}(q^2)}{\kappa_p - 1} \tag{71}$$

for nucleon resonances in the s channel and

$$F_{Y^\star}(q^2) = \frac{\tilde{F}_{2n}(q^2)}{\kappa_n} \tag{72}$$

for hyperon resonances in the u channel, where $\tilde{F}_{2p}$ and $\tilde{F}_{2n}$ are given by Eqs. (64) with the modified form-factor masses. Note that both form factors are normalized to unity at the physical photon point.

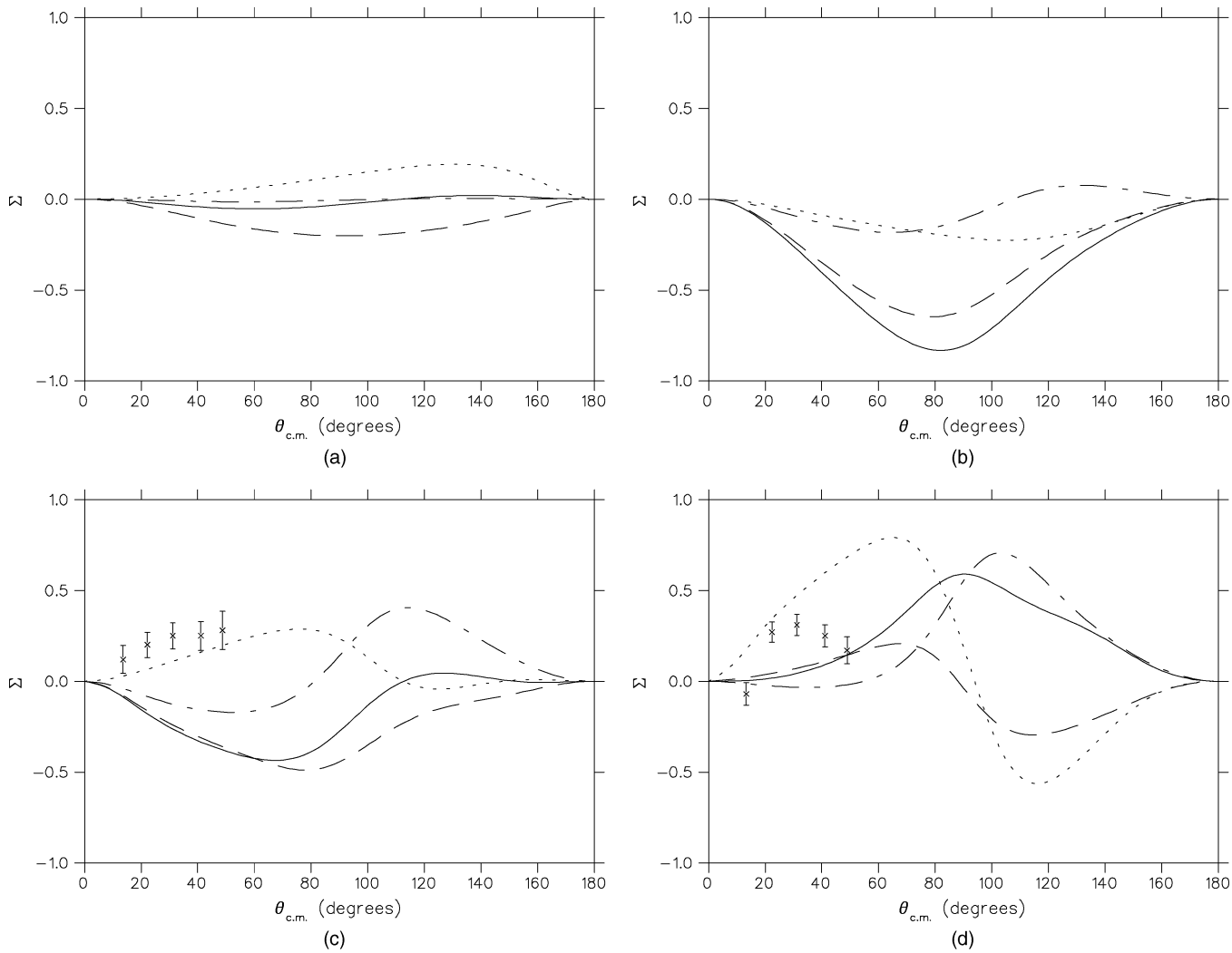

FIG. 5. Polarized photon beam asymmetry for the reaction $\gamma p \to K^+\Lambda$ at (a) $E_\gamma = 1.0$ GeV, (b) $E_\gamma = 1.25$ GeV, (c) $E_\gamma = 1.55$ GeV, and (d) $E_\gamma = 1.75$ GeV. Identification of curves as in Fig. 3. The data points are from Ref. [35].

IV. NUMERICAL RESULTS AND DISCUSSION

A. $\gamma p \to K^+\Lambda$

The quality of the various photoproduction fits is exhibited in Fig. 3, which displays the differential cross sections obtained with the four fits, along with the SAID empirical cross sections, at three different energies. It can be seen that all four fits yield good representations of the empirical cross sections over the full energy range considered.

Results for the three polarization parameters defined by Eqs. (33), (34), and (35) are presented in Figs. 4, 5, and 6 for several photon energies. The data points have been taken from a variety of sources, as indicated in the figures, and generally involve some energy averaging. It is apparent that the calculated polarization parameters vary considerably from one fit to another, despite the similarity of the corresponding cross sections. In fact, the variation exhibited here is more pronounced than that reported in Ref. [17], even though the cumulative χ^2 values obtained with the fits here are lower than those of the earlier work. Evidently, polarization data provide significant additional constraints on the photoproduction matrix elements that are not provided by the cross-section data alone.

As mentioned in the introduction, the available photoproduction polarization data have recently expanded quite considerably. Any model that seeks to quantitatively describe the photoproduction process certainly needs to incorporate this new data. In the present work, however, the emphasis is on studying the additional information that can be extracted from the electroproduction process as opposed to the photoproduction process. In the following subsection, it will be shown that the latter process may be able to provide important information regarding the electromagnetic form factors that cannot be extracted from the photoproduction process by itself.

B. $ep \to e'K^+\Lambda$

The virtual photoproduction cross section given by Eq. (52) is a function of five independent kinematic variables, which are conventionally selected to be the $K\Lambda$ center-of-mass energy

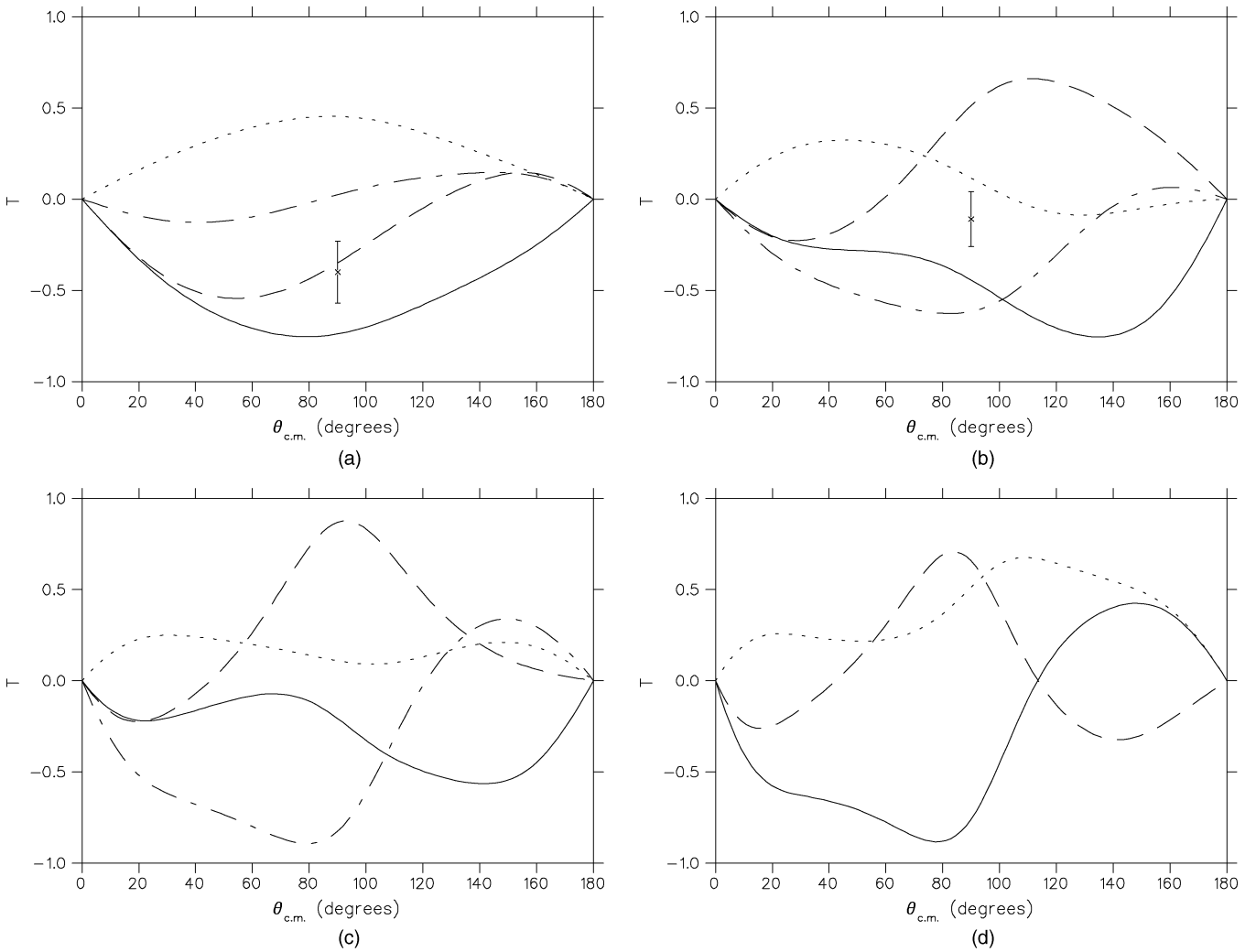

FIG. 6. Polarized proton target asymmetry for the reaction $\gamma p \to K^+\Lambda$ at (a) $E_\gamma = 1.1$ GeV, (b) $E_\gamma = 1.3$ GeV, (c) $E_\gamma = 1.55$ GeV, and (d) $E_\gamma = 1.7$ GeV. Identification of curves as in Fig. 3. The data points are from Ref. [36].

$W = \sqrt{s}$, the squared virtual photon four-momentum q^2, the transverse photon polarization ϵ, given by Eq. (41), the angle ϕ between the lepton and hadron planes, and either the kaon angle θ or the squared four-momentum transfer variable t. The ϵ and ϕ dependence of the cross section is shown explicitly in Eq. (52) so that each of the terms in that equation is a function of just three kinematic variables. In most of the previous theoretical studies of the virtual photoproduction of strangeness, the differential cross section with respect to t was examined. Here we examine the angular distribution of the cross section instead, because that is the quantity usually presented in experimental studies. As Eqs. (46) and (47) make clear, the two quantities are related by a kinematic factor that depends on both W and q^2.

Results for the unpolarized differential cross section as a function of $-q^2$ are presented in Fig. 7. The particular kinematics selected for these results were dictated in large measure by the available data. In general, the data points displayed in each panel do not correspond to exactly the same kinematics as the calculations. In particular, the values employed for θ and ϵ in the calculations represent compromises between the values associated with the various data points in each panel. Also, the data points from Ref. [3] were first scaled to the indicated energies using scaling functions provided in that reference and then converted from differential cross sections with respect to t to differential cross sections with respect to solid angle. The different curves in each panel correspond to the different photoproduction fits discussed in Sec. II and were all obtained with the form-factor multiplicative factor c_R set equal to unity. Although the different fits give somewhat different results, it can be seen that, except at low $-q^2$ for $W = 2.66$ GeV, the results are not dramatically different.

For lower values of W, our calculated results generally lie below the data and display a more rapid decrease with $-q^2$ than does the data. In comparison with previous theoretical studies, our results lie further away from the data. This is not surprising because no attempt has been made here to fit the model parameters to electroproduction data, in contrast with the fits presented in most of the earlier studies.

Similar conclusions regarding model dependence can be seen in Fig. 8, which exhibits results for the unpolarized differential cross section as a function of θ. Again, the different

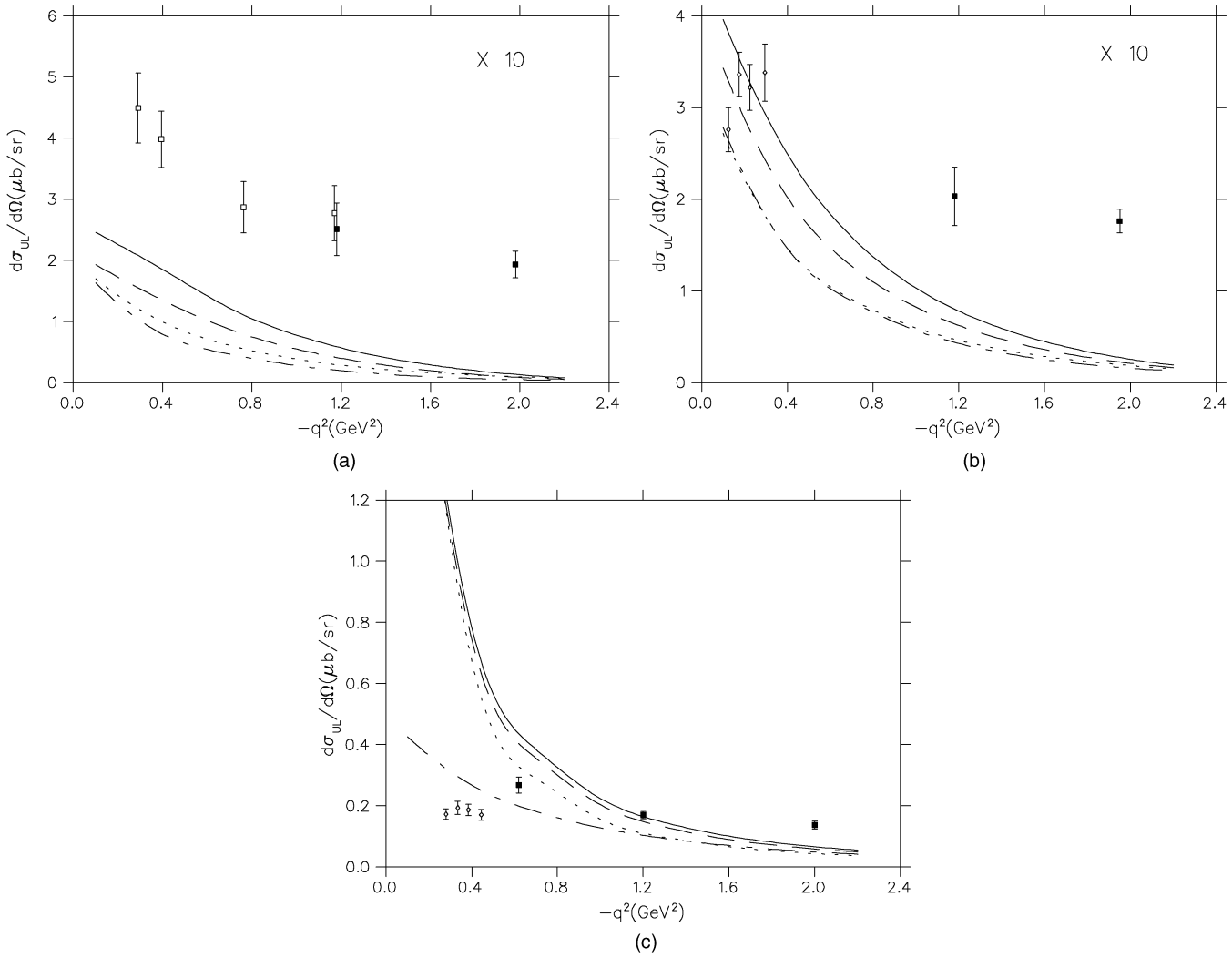

FIG. 7. Unpolarized differential cross section vs. $-q^2$ for the reaction $\gamma_v p \to K^+\Lambda$ at (a) $W = 2.165$ GeV, $\theta = 7.35^\circ$, and $\epsilon = 0.88$; (b) $W = 2.21$ GeV, $\theta = 15.2^\circ$, and $\epsilon = 0.80$; and (c) $W = 2.66$ GeV, $\theta = 12.1^\circ$, and $\epsilon = 0.765$. Identification of curves as described in the legend to Fig. 3. The data points are from Ref. [1] (open squares), Ref. [2] (solid squares), and Ref. [3] (open diamonds), as described in the text.

fits yield different results, but the differences are not very dramatic. Comparison with the data in this figure yields mixed conclusions. At lower W and small $-q^2$, the data generally lie above the calculated results, although, as seen in Fig. 8(b), the data from different references are not always consistent. At higher W and larger $-q^2$, the data and our calculated cross sections are closer together, but the paucity of data points makes a valid comparison difficult.

The calculated cross sections are compared with some more recent data in Fig. 9, where the unpolarized cross section is exhibited as a function of $-q^2$ for several values of ϵ. Again there is only modest model dependence on display here. At the low value of W for which these results were obtained, the calculated results lie well below the data, in agreement with the results exhibited in Fig. 7.

The sensitivity of the calculated cross sections to the form-factor parameter c_R is shown in Figs. 10, 11, and 12. In each of these figures, the two panels on the left exhibit results obtained with model A, whereas the two panels on the right exhibit results obtained with model D. In each panel the solid curve was obtained with $c_R = 1$, the dashed curve with a reduced value of c_R, and the remaining two curves with increased values of c_R. Note that reducing c_R from unity decreases the form-factor masses associated with s- and u-channel resonances and thereby enhances the transition form factors in comparison with the Born form factors. The variation of the calculated cross sections with c_R depends on both the photoproduction fit employed and the choice of kinematics. In Fig. 10, the results displayed for fit A vary much more with c_R than do the results displayed for fit D, which does not include spin $\frac{3}{2}$ resonances in the u channel. This can be seen in Fig. 11 as well, but in Fig. 12, which displays results obtained at a lower energy, the two fits yield cross sections with similar sensitivity to c_R. Comparison with the data in all three figures suggests that with an appropriate photoproduction model, it might be possible to fit the electroproduction data by just adjusting the resonance form factors. In Fig. 12, for example, it can be seen that simply increasing c_R from unity to the

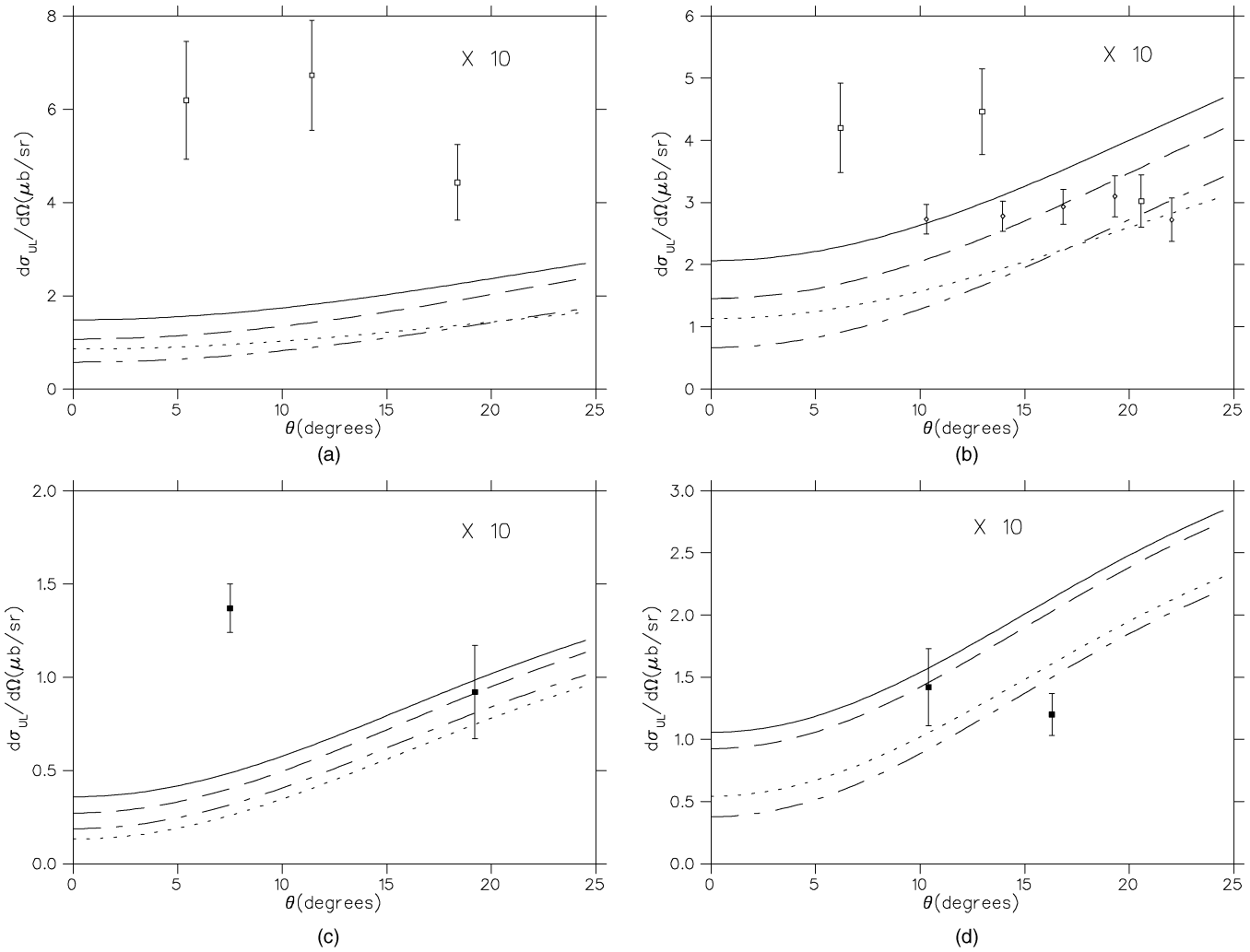

FIG. 8. Unpolarized differential cross section vs. θ for the reaction $\gamma_v p \to K^+\Lambda$ at (a) $W = 2.08$ GeV, $-q^2 = 0.415$ GeV^2, and $\epsilon = 0.89$; (b) $W = 2.26$ GeV, $-q^2 = 0.283$ GeV^2, and $\epsilon = 0.755$; (c) $W = 2.66$ GeV, $-q^2 = 2.02$ GeV^2, and $\epsilon = 0.85$; and (d) $W = 2.78$ GeV, $-q^2 = 1.39$ GeV^2, and $\epsilon = 0.875$. Identification of curves as described in the legend to Fig. 3. The data points are from Ref. [1] (open squares), Ref. [2] (solid squares), and Ref. [3] (open diamonds), as described in the text.

value 1.7 brings the calculated cross sections closer to the data.

Results for the different contributions to the cross section as defined by Eq. (52) are displayed in Fig. 13 for the four photoproduction fits described in Sec. II with $c_R = 1$ and in Fig. 14 for different values of c_R using fit A. Note that in these two figures, the cross section is expressed in nb rather than in μb. The data points for the longitudinal cross sections have been modified in both figures so as to be consistent with Eq. (52). Interestingly, it appears that the sensitivity of the calculated results to both the photoproduction fit employed and to the resonance form factors used depends on the particular cross section component considered, at least for the kinematics chosen here. This is especially evident in Fig. 14, which reveals that the form-factor sensitivity exhibited in Fig. 12 comes mainly from the $d\sigma_U$ component of the cross section.

In summary, we have studied the model dependence of $K\Lambda$ electroproduction from the proton using an effective Lagrangian model with parameters fit to $K\Lambda$ photoproduction cross sections. We have found that the virtual photoproduction cross sections show some dependence on the photoproduction fit employed but that the calculated results are far more sensitive to the treatment of the s- and u-channel transition form factors. By adjusting a single resonance form-factor parameter, we were able to move our calculated cross sections closer to the data for a variety of kinematical choices. This suggests that electroproduction data, in conjunction with a reaction model fit quantitatively to photoproduction data, can provide significant information concerning the electromagnetic transition form factors.

APPENDIX: AMPLITUDE COEFFICIENTS

The amplitude coefficients appearing in Eq. (51) depend on both the channel considered and the spin and parity of the intermediate baryon or meson. Here we give detailed expressions for the nonzero coefficients associated with the various contributions in each channel.

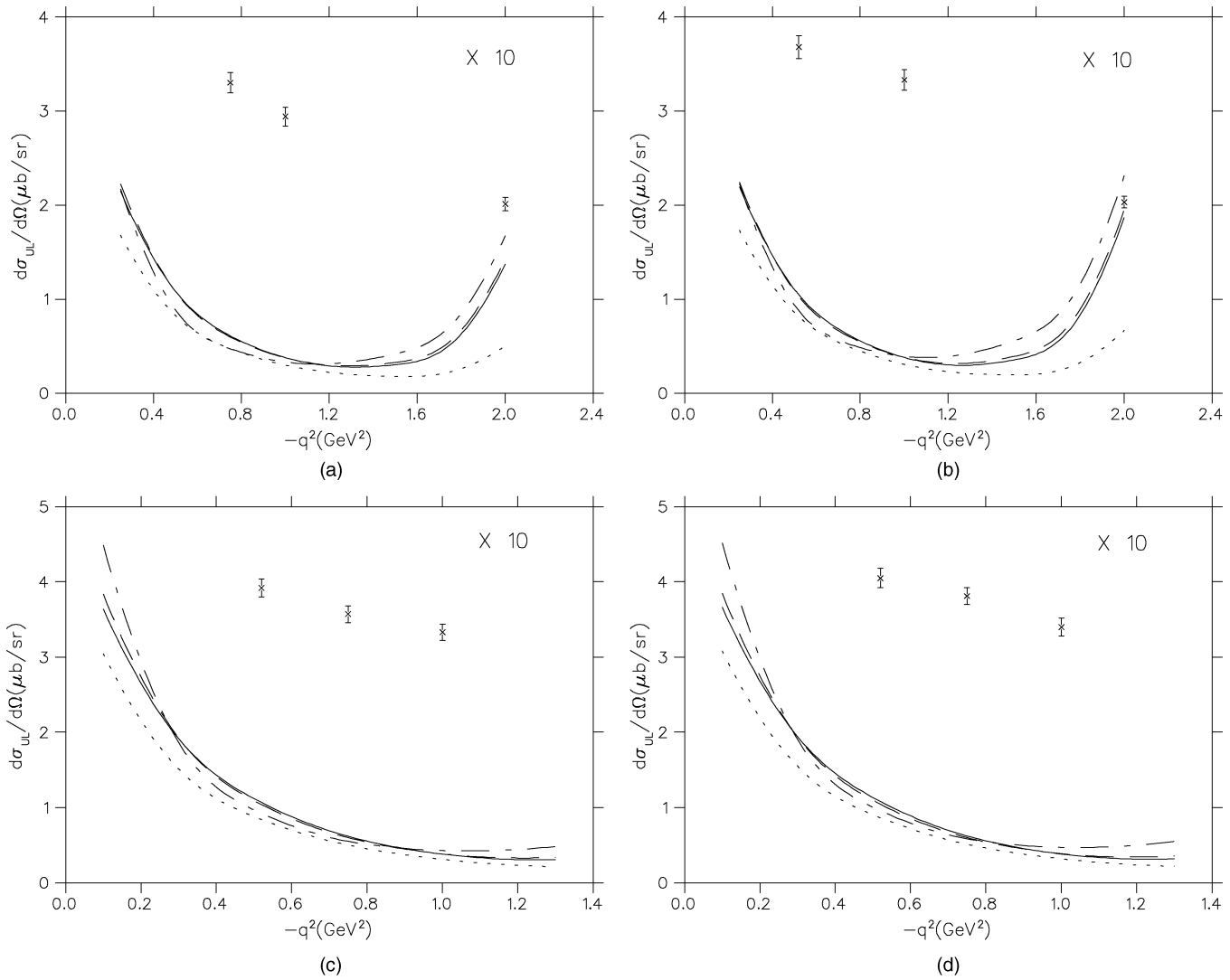

FIG. 9. Unpolarized differential cross section vs. $-q^2$ for the reaction $\gamma_v p \to K^+\Lambda$ at $W = 1.83$ GeV, $\theta = 0^\circ$, and (a) $\epsilon = 0.44$, (b) $\epsilon = 0.61$, (c) $\epsilon = 0.72$, and (d) $\epsilon = 0.84$. Identification of curves as describe in the legend to Fig. 3. The data points are from Ref. [6].

We begin by defining products of the coupling strengths, Dirac normalization factors, and intermediate propagator denominators. In particular, for the t channel, we define

$$\begin{aligned} F_t &= N_p N_\Lambda F_K d(t) \\ G_{t1} &= N_p N_\Lambda \frac{G^V_{K^\star}}{m_{\rm sc}} d(t) \\ G_{t2} &= N_p N_\Lambda \frac{G^T_{K^\star}}{m_{\rm sc}(m_\Lambda + m_p)} d(t) \end{aligned} \tag{A1}$$

with N_p and N_Λ defined by Eq. (30), the coupling products defined by Eqs. (22) and (23), and the propagator denominators defined by

$$d(t) = \left(t - m_I^2 + i m_I \Gamma_I\right)^{-1}, \tag{A2}$$

where m_I and Γ_I are the mass and width of the intermediate meson. With $N^\star$ and $Y^\star$ referring to any of the intermediate baryons exchanged in the s and u channels, respectively, the corresponding s- and u-channel expressions are

$$\begin{aligned} F_s &= N_p N_\Lambda \frac{F_{N^\star}}{2m_p} d(s) \\ F_{sC} &= N_p N_\Lambda F_{Cp} d(s) \\ G_{s1} &= N_p N_\Lambda \frac{G^1_{N^\star}}{2m_p m_\pi} d(s) \\ G_{s2} &= N_p N_\Lambda \frac{G^2_{N^\star}}{(2m_p)^2 m_\pi} d(s) \end{aligned} \tag{A3}$$

and

$$\begin{aligned} F_u &= N_p N_\Lambda \frac{F_{Y^\star}}{2m_\Lambda} d(u) \\ F_{uC} &= N_p N_\Lambda F_{CY} d(u) \\ G_{u1} &= N_p N_\Lambda \frac{G^1_{Y^\star}}{2m_\Lambda m_\pi} d(u) \\ G_{u2} &= N_p N_\Lambda \frac{G^2_{Y^\star}}{(2m_\Lambda)^2 m_\pi} d(u) \end{aligned} \tag{A4}$$

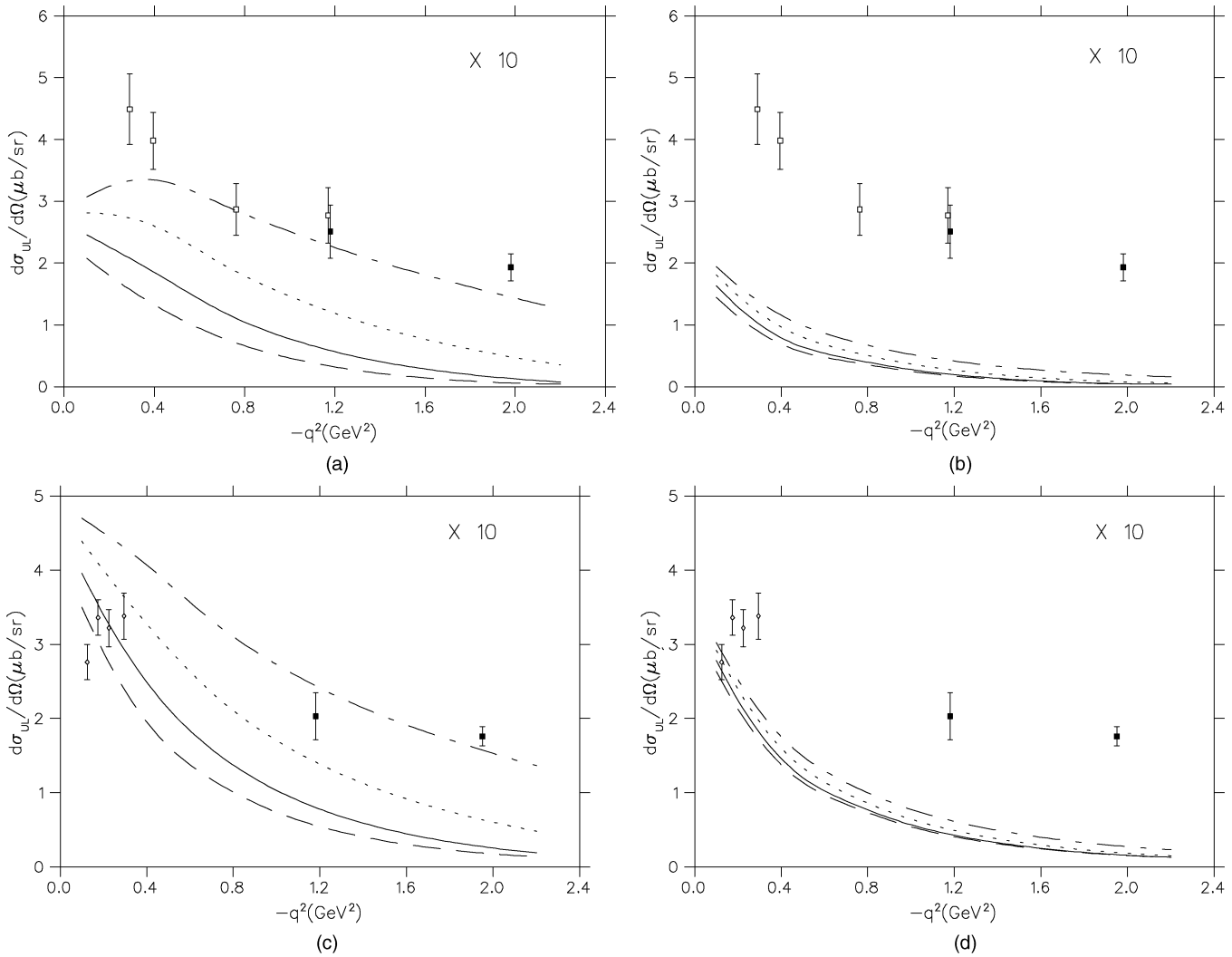

FIG. 10. Unpolarized differential cross section vs. $-q^2$ for the reaction $\gamma_v p \to K^+\Lambda$ at (a) $W = 2.165$ GeV, $\theta = 7.35^\circ$, and $\epsilon = 0.88$ using model A; (b) $W = 2.165$ GeV, $\theta = 7.35^\circ$, and $\epsilon = 0.88$ using model D; (c) $W = 2.21$ GeV, $\theta = 15.2^\circ$, and $\epsilon = 0.80$ using model A; and (d) $W = 2.21$ GeV, $\theta = 15.2^\circ$, and $\epsilon = 0.80$ using model D. The solid cureves were obtained with $c_R = 1.0$, the dashed curves with $c_R = 0.8$, the dotted curves with $c_R = 1.3$, and the dot-dashed curves with $c_R = 1.7$. The data points are from Ref. [1] (open squares), Ref. [2] (solid squares), and Ref. [3] (open diamonds), as described in the text.

with the coupling products defined by Eqs. (20), (21), and (24) and the propagator denominators defined by expressions analogous to Eq. (A2). Note that $\Gamma_I = 0$ in all the Born terms and in the u-channel resonance contributions.

With these definitions, we then have in the t channel

$$\begin{aligned} B_2 &= -2B_1 = 2F_t(E_p + m_p) \\ C_2 &= -2C_1 = -2F_t(E_\Lambda + m_\Lambda) \end{aligned} \tag{A5}$$

for the Born term,

$$\begin{aligned} B_1 &= -H_+\mathcal{E}_\Lambda q_0 \\ B_2 &= H_+\mathcal{E}_p q_0 \\ C_1 &= H_+\mathcal{E}_\Lambda E_K \\ C_2 &= -H_+\mathcal{E}_p E_K \\ D &= -(B_1 + C_2)\mathbf{p_K}\cdot\mathbf{q} - C_1|\mathbf{q}|^2 - B_2|\mathbf{p_K}|^2 \end{aligned}$$

$$\begin{aligned} E &= H_+ + 2G_{t2}\sqrt{s} \\ A &= (H_+ - 2G_{t2}\sqrt{s})\mathcal{E}_\Lambda\mathcal{E}_p + E\mathbf{p_K}\cdot\mathbf{q} - (B_1 + C_2) \end{aligned} \tag{A6}$$

for an intermediate $K(892)$ resonance and

$$\begin{aligned} A &= H_-\left(q_\mu p_K^\mu - q^2\right) \\ B_1 &= \mathcal{E}_p\left[H_-(\sqrt{s} - m_p) + 2G_{t2}q_\mu p_\Lambda^\mu\right] - A \\ B_2 &= -\mathcal{E}_p\left[H_-(\sqrt{s} - m_p) + 2G_{t2}q_\mu p_p^\mu\right] \\ C_1 &= \mathcal{E}_\Lambda\left[H_-(\sqrt{s} + m_p) - 2G_{t2}q_\mu p_\Lambda^\mu\right] \\ C_2 &= -\mathcal{E}_\Lambda\left[H_-(\sqrt{s} + m_p) - 2G_{t2}q_\mu p_p^\mu\right] - A \\ D &= A(\mathbf{p_K}\cdot\mathbf{q} - \mathcal{E}_\Lambda\mathcal{E}_p) \end{aligned} \tag{A7}$$

for an intermediate $K(1270)$ resonance, where

$$\mathcal{E} = E + m \tag{A8}$$

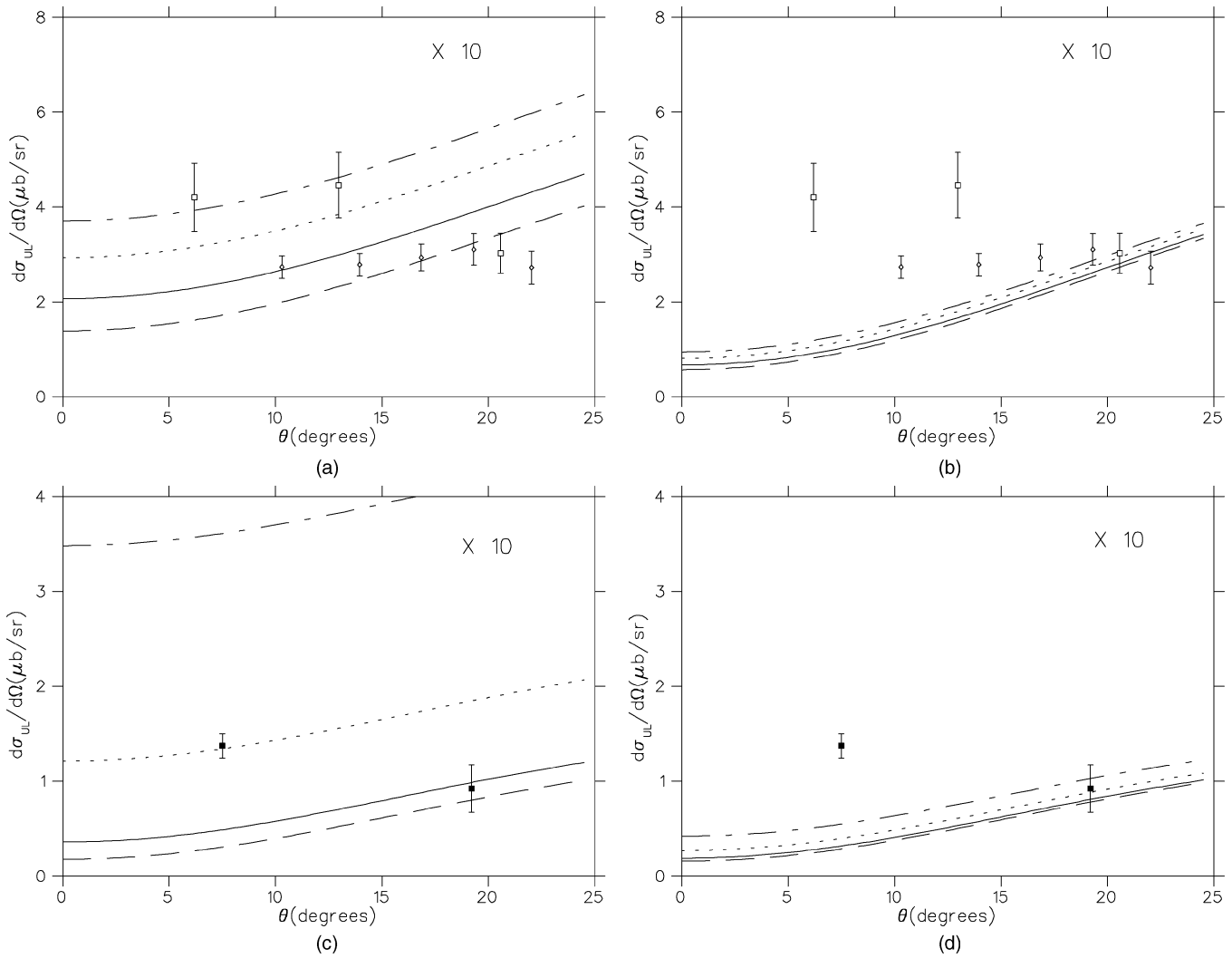

FIG. 11. Unpolarized differential cross section vs. θ for the reaction $\gamma_v p \to K^+\Lambda$ at (a) $W = 2.26$ GeV, $-q^2 = 0.283$ GeV^2, and $\epsilon = 0.755$ using model A; (b) $W = 2.26$ GeV, $-q^2 = 0.283$ GeV^2, and $\epsilon = 0.755$ using model D; (c) $W = 2.66$ GeV, $-q^2 = 2.02$ GeV^2, and $\epsilon = 0.85$ using model A; and (d) $W = 2.66$ GeV, $-q^2 = 2.02$ GeV^2, and $\epsilon = 0.85$ using model D. Identification of curves as described in the legend to Fig. 10. The data points are from Ref. [1] (open squares), Ref. [2] (solid squares), and Ref. [3] (open diamonds), as described in the text.

and

$$H_\pm = G_{t1} + G_{t2}(m_\Lambda \pm m_p). \tag{A9}$$

In the s channel, we have

$$\begin{aligned} A &= -C_2 = F_{sC}(\sqrt{s} + m_p) + F_s(\sqrt{s} + m_p)^2 \\ B_1 &= -(F_{sC} + F_s q_0)(\sqrt{s} + m_p) \\ C_1 &= F_s \mathcal{E}_\Lambda(\sqrt{s} - m_p) \\ D &= F_{sC}\mathcal{E}_\Lambda \mathcal{E}_p(\sqrt{s} - m_p) + A\mathbf{p_K}\cdot\mathbf{q} - C_1(\mathcal{E}_p q_0 + |\mathbf{q}|^2) \end{aligned} \tag{A10}$$

for the Born term, including the charge-coupling contribution,

$$\begin{aligned} A &= -C_2 = F_s(\sqrt{s} + m_p)(m_I \pm \sqrt{s}) \\ B_1 &= -F_s q_0(m_I \pm \sqrt{s}) \\ C_1 &= -F_s \mathcal{E}_\Lambda(m_I \mp \sqrt{s}) \\ D &= A\mathbf{p_K}\cdot\mathbf{q} - C_1(\mathcal{E}_p q_0 + |\mathbf{q}|^2) \end{aligned} \tag{A11}$$

for an intermediate $\frac{1}{2}^\pm$ resonance, where m_I is the intermediate resonance mass, and

$$\begin{aligned} A &= -\tfrac{1}{3}G_{s2}\alpha_p\beta_\pm + G_{s1}\alpha_K(\sqrt{s} \mp m_I) \\ B_1 &= (G_{s2}\mathcal{E}_p \pm G_{s1})\alpha_K(m_I \mp \sqrt{s}) - \tfrac{1}{3}G_{s2}m_p q_0 \beta_\pm \\ B_2 &= \left[G_{s2}\alpha_p\mathcal{E}_p \pm G_{s1}(\alpha_p + m_p q_0)\right](m_I \mp \sqrt{s}) \\ C_1 &= G_{s2}\left[\tfrac{1}{3}\Omega_\pm(\sqrt{s} + m_p) - \alpha_K\mathcal{E}_\Lambda(m_I \pm \sqrt{s})\right] \\ C_2 &= -A - \left[G_{s2}\alpha_p \mp G_{s1}(\sqrt{s} + m_p)\right]\mathcal{E}_\Lambda(m_I \pm \sqrt{s}) \\ D &= A\mathbf{p_K}\cdot\mathbf{q} + \left[-\tfrac{1}{3}G_{s2}\alpha_p\Omega_\pm + G_{s1}\alpha_K\mathcal{E}_\Lambda(\sqrt{s} \pm m_I)\right]\mathcal{E}_p \end{aligned} \tag{A12}$$

for an intermediate $\frac{3}{2}^\pm$ resonance, where

$$\alpha_p = E_p q_0 + |\mathbf{q}|^2, \tag{A13}$$

$$\alpha_K = \left(1 - \frac{2s}{3m_I^2}\right)E_K q_0 - \mathbf{p_K}\cdot\mathbf{q}, \tag{A14}$$

$$\beta_\pm = \mathcal{E}_\Lambda(m_I \pm \sqrt{s}) + E_K(m_I \mp \sqrt{s}), \tag{A15}$$

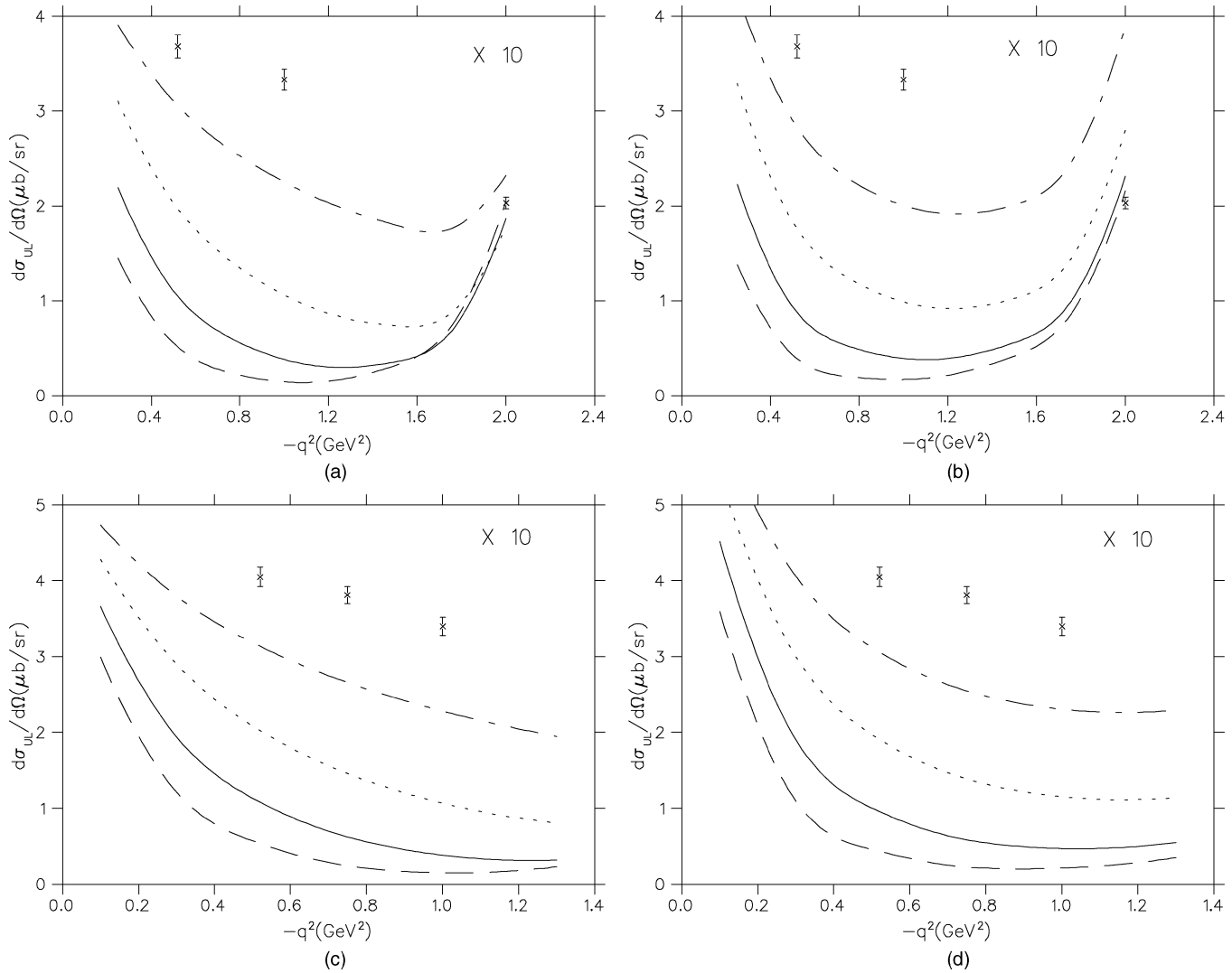

FIG. 12. Unpolarized differential cross section vs. $-q^2$ for the reaction $\gamma_v p \to K^+\Lambda$ at $W = 1.83$ GeV, $\theta = 0^\circ$, and (a) $\epsilon = 0.61$ using model A; (b) $\epsilon = 0.61$ using model D; (c) $\epsilon = 0.84$ using model A; and (d) $\epsilon = 0.84$ using model D. Identification of curves as described in the legend to Fig. 10. The data points are from Ref. [6].

and

$$\Omega_\pm = E_K \mathcal{E}_\Lambda (m_I \pm \sqrt{s}) + |\mathbf{p_K}|^2 (m_I \mp \sqrt{s}). \quad \text{(A16)}$$

Finally, in the u channel,

$$\begin{aligned} A &= F_{uC}(\sqrt{s} - \Delta m) + F_u[s_{p+}(m_Y + m_\Lambda) - \alpha_+] \\ B_1 &= -A + F_u \mathcal{E}_p(\sqrt{s} + m_Y + m_\Lambda - m_p) \\ B_2 &= 2(-F_{uC} + F_u s_{p-})\mathcal{E}_p \\ C_1 &= F_u \mathcal{E}_\Lambda(\sqrt{s} - m_Y - m_\Lambda + m_p) \\ C_2 &= -A + 2(F_{uC} + F_u s_{p+})\mathcal{E}_\Lambda \\ D &= F_{uC}\mathcal{E}_\Lambda \mathcal{E}_p(\sqrt{s} + \Delta m) + A\mathbf{p_K}\cdot\mathbf{q} \\ &\quad + F_u \mathcal{E}_\Lambda \mathcal{E}_p[\alpha_+ + s_{p-}(m_Y + m_\Lambda)] \end{aligned} \quad \text{(A17)}$$

for the Born terms with

$$\Delta m = m_Y - m_p - m_\Lambda, \quad \text{(A18)}$$

$$s_{p\pm} = \sqrt{s} \pm m_p, \quad \text{(A19)}$$

and

$$\alpha_\pm = \pm\left(q_\mu q^\mu - 2q_\mu p_\Lambda^\mu\right), \quad \text{(A20)}$$

$$\begin{aligned} A &= F_u[s_{p+}(m_I \pm m_\Lambda) - \alpha_\pm] \\ B_1 &= -A + F_u \mathcal{E}_p[m_I \pm (\sqrt{s} + m_\Lambda - m_p)] \\ B_2 &= \pm 2F_u \mathcal{E}_p s_{p-} \\ C_1 &= -F_u \mathcal{E}_\Lambda[m_I \pm (-\sqrt{s} + m_\Lambda - m_p)] \\ C_2 &= -A \pm 2F_u \mathcal{E}_\Lambda s_{p+} \\ D &= A\mathbf{p_K}\cdot\mathbf{q} + F_u \mathcal{E}_\Lambda \mathcal{E}_p[\alpha_\pm + s_{p-}(m_I \pm m_\Lambda)] \end{aligned} \quad \text{(A21)}$$

for an intermediate $\frac{1}{2}^\pm$ resonance, and

$$\begin{aligned} A &= (a_3 + a_4 s_{p+})s_{\Lambda+} - a_1 - a_2 s_{p+} \\ B_1 &= -A + \mathcal{E}_p[b_1 - b_2 s_{p-} + (b_4 s_{p-} - b_3)s_{\Lambda+}] \\ B_2 &= \mathcal{E}_p[c_1 - c_2 s_{p-} + (c_4 s_{p-} - c_3)s_{\Lambda+}] \\ C_1 &= -\mathcal{E}_\Lambda[b_1 + b_2 s_{p+} + (b_4 s_{p+} + b_3)s_{\Lambda-}] \end{aligned}$$

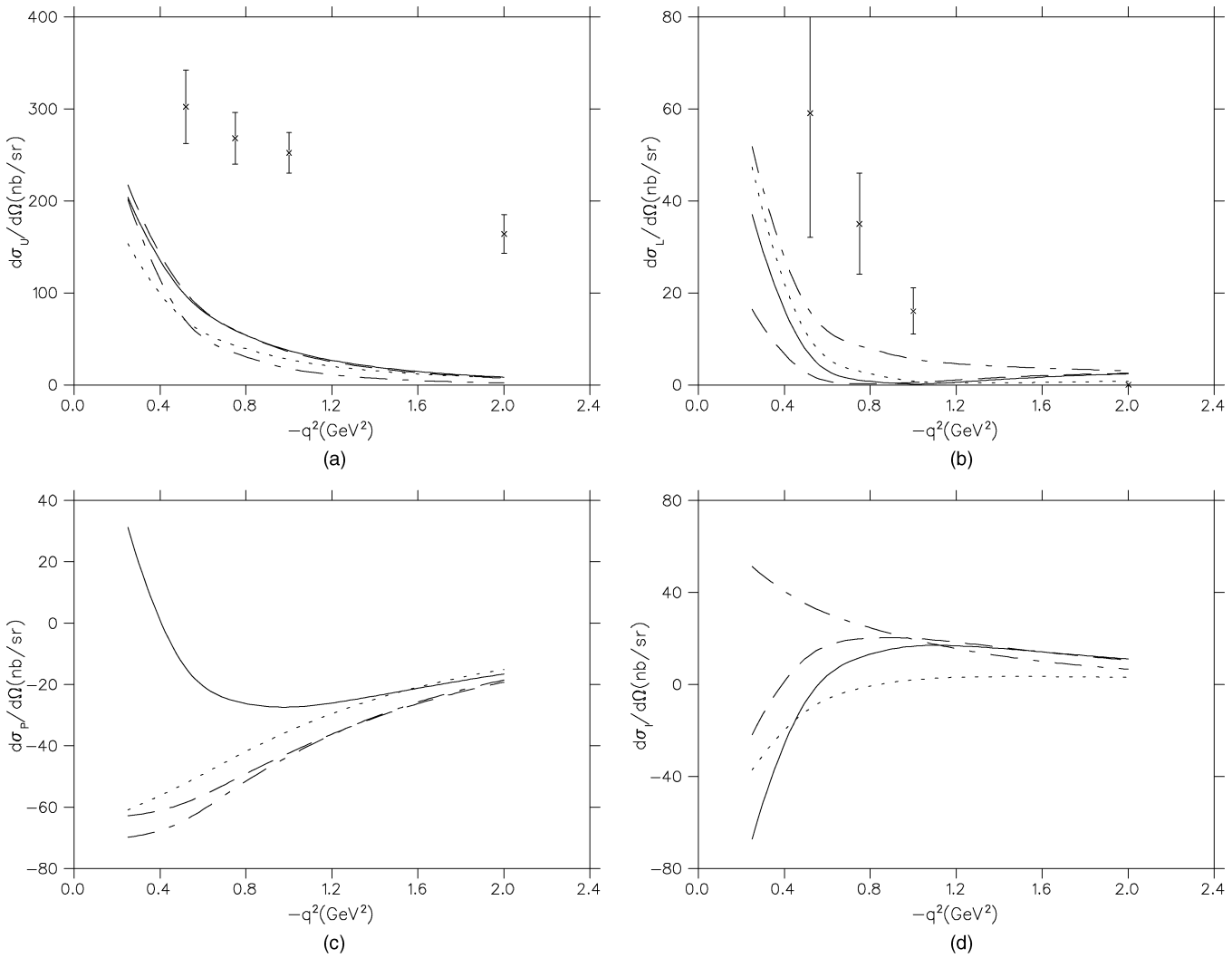

FIG. 13. (a) $d\sigma_U/d\Omega_K$ vs. $-q^2$, (b) $d\sigma_L/d\Omega_K$ vs. $-q^2$, (c) $d\sigma_P/d\Omega_K$ vs. $-q^2$, and (d) $d\sigma_I/d\Omega_K$ vs. $-q^2$ for the reaction $\gamma_v p \to K^+\Lambda$ at $W = 1.83$ GeV and $\theta = 0^\circ$. Identification of curves as described in the legend to Fig. 3. The data points are from Ref. [6], as described in the text.

$$C_2 = -A - \mathcal{E}_\Lambda[c_1 + c_2 s_{p+} + (c_4 s_{p+} + c_3)s_{\Lambda-}]$$
$$D = A\mathbf{p_K}\cdot\mathbf{q} + \mathcal{E}_\Lambda\mathcal{E}_p[a_1 - a_2 s_{p-} + (a_3 - a_4 s_{p-})s_{\Lambda-}] \tag{A22}$$

for an intermediate $\frac{3}{2}^\pm$ resonance with

$$s_{\Lambda\pm} = \sqrt{s} \pm m_\Lambda, \tag{A23}$$
$$a_1 = \pm(G_{u1}m_\pm + G_{u2}p_\Lambda\cdot q)p_K\cdot q \pm 2G_{u1}\frac{p_\Lambda\cdot q p_K\cdot q - p_\Lambda\cdot p_K q^2}{m_I} \pm G_{u2}p_\Lambda\cdot p_K p_\Lambda\cdot q + \left(2G_{u1}\frac{p_I\cdot q}{m_I} - G_{u2}p_\Lambda\cdot q\right)\frac{m_\Lambda}{m_I}p_I\cdot p_K$$
$$a_2 = -G_{u1}(2p_\Lambda\cdot p_K + p_K\cdot q) \mp 2G_{u1}\frac{m_\Lambda}{m_I}p_I\cdot p_K + \left(2G_{u1}\frac{p_I\cdot q}{m_I} - G_{u2}p_\Lambda\cdot q\right)\frac{p_I\cdot p_K}{m_I}$$
$$a_3 = -G_{u1}m_\pm\frac{p_I\cdot q}{m_I} + (G_{u2}m_\mp - 2G_{u1})p_\Lambda\cdot q$$
$$a_4 = \pm G_{u1}\left(2m_\pm + \frac{p_I\cdot q}{m_I}\right) \pm G_{u2}p_\Lambda\cdot q, \tag{A24}$$

$$b_1 = 2(G_{u1}m_\pm + G_{u2}p_\Lambda\cdot q)\frac{p_\Lambda\cdot p_K}{m_I} + 2[G_{u1}q^2 + (G_{u2}m_\mp - 2G_{u1})p_\Lambda\cdot q]\frac{p_I\cdot p_K}{m_I^2}$$
$$b_2 = \pm 2(G_{u1}m_\pm + G_{u2}p_\Lambda\cdot q)\frac{p_I\cdot p_K}{m_I^2} \tag{A25}$$
$$b_3 = \pm G_{u1}\left(\frac{q^2 - 2p_\Lambda\cdot q}{m_I} - 2m_\pm\right) \mp G_{u2}m_\pm\frac{p_\Lambda\cdot q}{m_I}$$
$$b_4 = -\frac{1}{m_I}(G_{u1}m_\pm + G_{u2}p_\Lambda\cdot q),$$

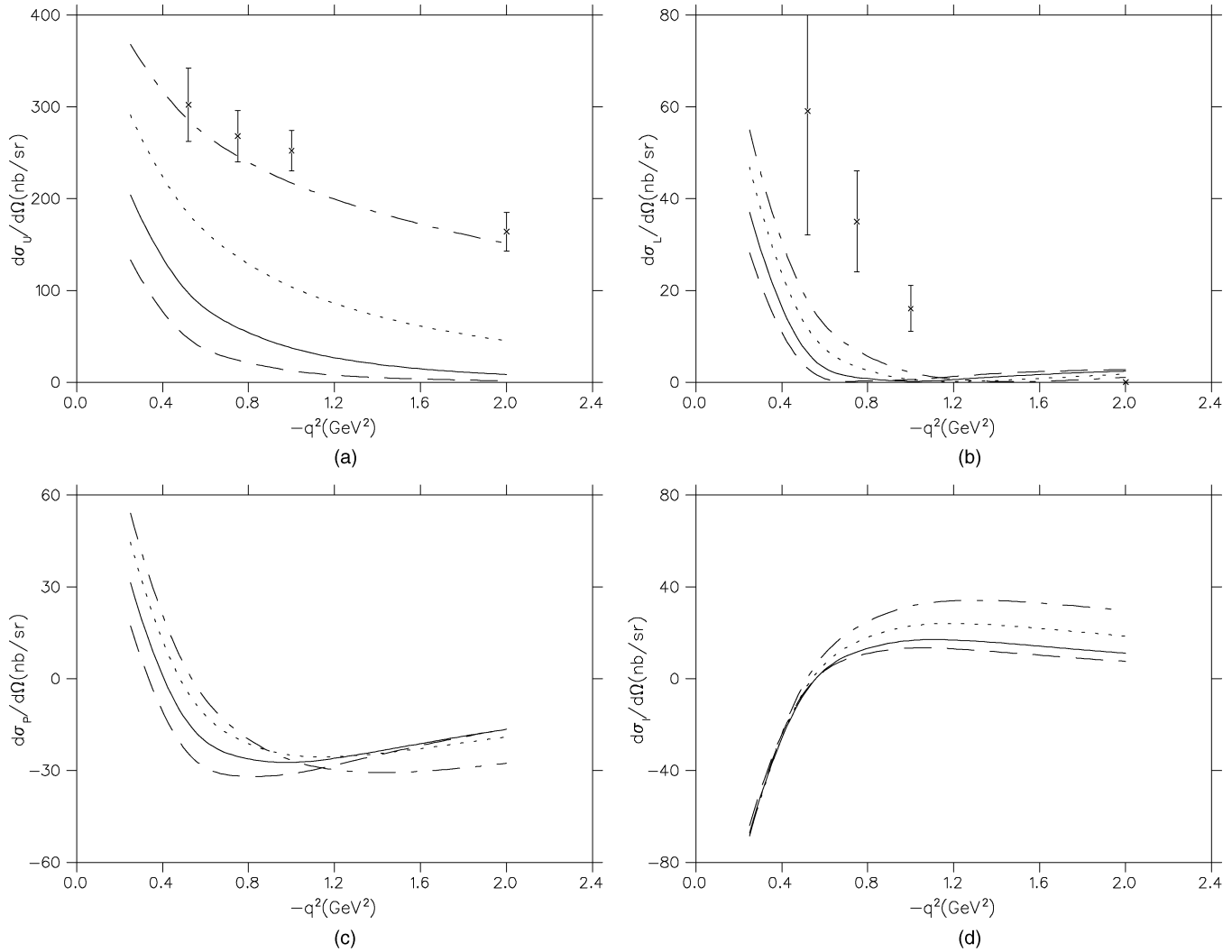

FIG. 14. (a) $d\sigma_U/d\Omega_K$ vs. $-q^2$, (b) $d\sigma_L/d\Omega_K$ vs. $-q^2$, (c) $d\sigma_P/d\Omega_K$ vs. $-q^2$, and (d) $d\sigma_I/d\Omega_K$ vs. $-q^2$ for the reaction $\gamma_v p \to K^+\Lambda$ at $W = 1.83$ GeV and $\theta = 0^\circ$ using model A. Identification of curves as described in the legend to Fig. 10. The data points are from Ref. [6], as described in the text.

and

$$c_1 = G_{u2} m_\mp \sqrt{s} q_0 + G_{u1} q^2 + 2(G_{u2} m_\mp - G_{u1}) \frac{p_I \cdot p_K}{m_I^2} q^2 + G_{u2} \frac{p_\Lambda \cdot p_K + p_K \cdot q}{m_I} q^2 \pm 2 G_{u1} \frac{m_\Lambda}{m_I} p_p \cdot q$$

$$c_2 = \pm(G_{u2}\sqrt{s} q_0 - G_{u1} m_\pm) \pm G_{u2} \left(2 p_K \cdot q + m_\mp \frac{p_I \cdot p_K}{m_I} \right) \pm 2 G_{u1} \frac{p_K \cdot q - p_p \cdot q}{m_I} + 2(G_{u1} m_\Lambda \pm G_{u2} q^2) \frac{p_I \cdot p_K}{m_I^2}$$

$$c_3 = (-G_{u2} m_\Lambda \mp G_{u1}) \frac{q^2}{m_I}$$

$$c_4 = -G_{u1} \left(2 + \frac{m_\pm}{m_I} \right) + G_{u2} \left(m_\pm - \frac{q^2}{m_I} \right), \qquad \text{(A26)}$$

where now the p's designate the corresponding four-momenta and

$$m_\pm = m_I \pm m_\Lambda. \qquad \text{(A27)}$$

[1] C. N. Brown, C. R. Canizares, W. E. Cooper, A. M. Eisner, G. J. Feldman, C. A. Lichtenstein, L. Litt, W. Lockeretz, V. B. Montana, F. M. Pipkin, and N. Hicks, Phys. Rev. Lett. **28**, 1086 (1972).

[2] C. J. Bebek, C. N. Brown, M. Herzlinger, S. Holmes, C. A. Lichtenstein, F. M. Pipkin, L. K. Sisterson, D. Andrews, K. Berkelman, D. G. Cassel, D. L. Hartill, and N. Hicks, Phys. Rev. Lett. **32**, 21 (1974); C. J. Bebek, C. N. Brown, P. Bucksbaum, M. Herzlinger, S. D. Holmes, C. A. Lichtenstein, F. M. Pipkin, S. W. Raither, and L. K. Sisterson, Phys. Rev. D **15**, 594 (1977).

[3] T. Azemoon, I. Dammann, C. Driver, D. Luke, G. Specht, K. Heinloth, H. Ackermann, E. Ganssauge, F. Janata, and D. Schmidt, Nucl. Phys. **B95**, 77 (1975).

[4] G. Niculescu *et al*., Phys. Rev. Lett. **81**, 1805 (1998).
[5] L. Teodorescu *et al*., Nucl. Phys. **A658**, 362 (1999).
[6] R. M. Mohring *et al*., Phys. Rev. C **67**, 055205 (2003).
[7] D. S. Carman *et al*., Phys. Rev. Lett. **90**, 131804 (2003).
[8] N. Levy, W. Majerotto, and B. J. Read, Nucl. Phys. **B55**, 493 (1973); **B55**, 513 (1973); A. Bartl and W. Majerotto, *ibid*. **B90**, 285 (1975).
[9] R. A. Adelseck and L. E. Wright, Phys. Rev. C **38**, 1965 (1988).
[10] R. A. Williams, Chueng-Ryon Ji, and Stephen R. Cotanch, Phys. Rev. C **46**, 1617 (1992).
[11] J. C. David, C. Fayard, G. H. Lamot, and B. Saghai, Phys. Rev. C **53**, 2613 (1996).
[12] T. Mizutani, C. Fayard, G.-H. Lamot, and B. Saghai, Phys. Rev. C **58**, 75 (1998).
[13] H. Haberzettl, C. Bennhold, and T. Mart, Nucl. Phys. **A684**, 475c (2001).
[14] M. Vanderhaeghen, M. Guidal, and J.-M. Laget, Phys. Rev. C **57**, 1454 (1998); M. Guidal, J.-M. Laget, and M. Vanderhaeghen, *ibid*. **61**, 025204 (2000); **68**, 058201 (2003).
[15] S. Janssen, J. Ryckebusch, and T. Van Cauteren, Phys. Rev. C **67**, 052201(R) (2003).
[16] T. Mart and C. Bennhold, Nucl. Phys. **A639**, 237c (1998).
[17] O. V. Maxwell, Phys. Rev. C **70**, 044612 (2004).
[18] R. A. Adelseck, C. Bennhold, and L. E. Wright, Phys. Rev. C **32**, 1681 (1985).
[19] O. V. Maxwell, Phys. Rev. C **69**, 034605 (2004).
[20] C. Caso *et al*., Eur. Phys. J. C **3**, 1 (1998).
[21] M. Benmerrouche, R. M. Davidson, and Nimai C. Mukhopadhyay, Phys. Rev. C **39**, 2339 (1989).
[22] J. J. de Swart, Rev. Mod. Phys. **35**, 916 (1963).
[23] CNS Data Analysis Center web site; J. S. Hyslop, R. A. Arndt, L. D. Roper, and R. L. Workman, Phys. Rev. D **46**, 961 (1992).
[24] B. Saghai, Nucl. Phys. **A639**, 217c (1998).
[25] F. Cardarelli, I. L. Grach, I. M. Narodetskii, E. Pace, G. Salme, and S. Simula, Phys. Rev. D **53**, 6682 (1996).
[26] M. Gari and W. Krumpelmann, Z. Phys. A **322**, 689 (1985); M. Gari and W. Krumpelmann, Phys. Lett. **B173**, 10 (1986); M. F. Gari and W. Krumpelmann, Phys. Rev. D **45**, 1817 (1992).
[27] H. C. Kim, A. Blotz, M. V. Polyakov, and K. Goeke, Phys. Rev. D **53**, 4013 (1996).
[28] R. A. Williams and C. Puckett-Truman, Phys. Rev. C **53**, 1580 (1996); R. A. Williams and T. M. Small, *ibid*. **55**, 882 (1997).
[29] H. Thom, E. Gabathuler, D. Jones, B. D. McDaniel, and W. M. Woodward, Phys. Rev. Lett. **11**, 433 (1963).
[30] M. Grilli, L. Mezzetti, M. Nigro, and E. Schiavuta, Nuovo Cimento **38**, 1467 (1965).
[31] T. Fujii *et al*., Phys. Rev. D **2**, 439 (1970).
[32] D. E. Groom and J. H. Marshall, Phys. Rev. **159**, 1213 (1967).
[33] R. Hass, T. Miczaika, U. Opara, K. Quabach, and W. J. Schwille, Nucl. Phys. **B137**, 261 (1978).
[34] M. Q. Tran *et al*., Phys. Lett. **B445**, 20 (1998); S. Goers *et al*., *ibid*. **B464**, 331 (1999).
[35] R. G. T. Zegers *et al*., Phys. Rev. Lett. **91**, 092001 (2003).
[36] K. H. Althoff *et al*., Nucl. Phys. **B137**, 269 (1978).